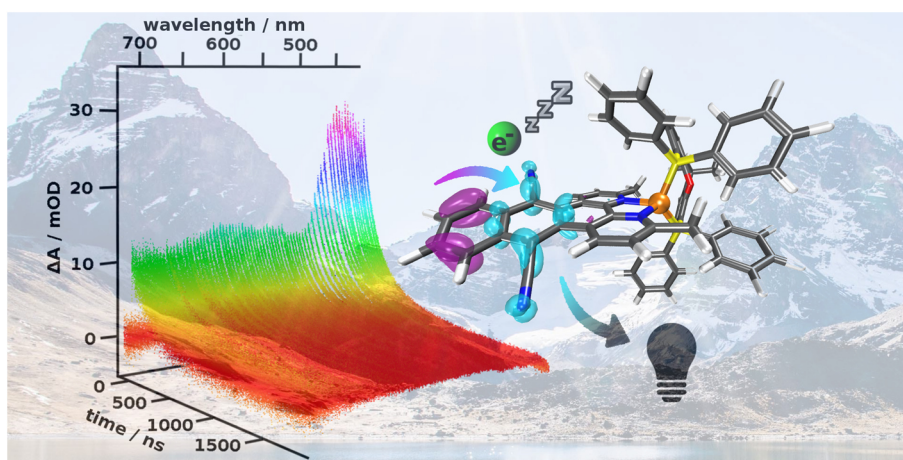# Electronic Supplementary Information

Remarkably long-lived excited states of copper photosensitizers containing an extended π–system based on an anthracene moiety

Robin Giereth,[a,†] Immanuel Reim,[b,†] Wolfgang Frey,[b] Henrik Junge,[c] Stefanie Tschierlei[*a] and Michael Karnahl[*b]

* Corresponding authors: Dr. Stefanie Tschierlei, E-mail: stefanie.tschierlei@uni-ulm.de
Dr. Michael Karnahl, E-mail: michael.karnahl@oc.uni-stuttgart.de

Electronic Supplementary Information - Table of Contents

1 Experimental Details

NMR spectra were recorded on a Bruker Avance III HD 400 at 293 K and processed with MestReNova software (Version 12.0.0). The chemical shifts δ are reported in parts per million (ppm). ^{1}H- and ^{13}C-NMR shifts are referenced according to the applied deuterated solvent as internal standard.[1] ^{31}P{^{1}H}-NMR shifts are proton decoupled and given relatively to H_3PO_4 (85 %, δ = 0 ppm) as an external reference. Coupling constants J are presented as absolute values in Hz, without considering the kind of the coupling. For the characterization of the NMR signals the following abbreviations are used: s = singlet, d = doublet, t = triplet, q = quartet, m = multiplet and dd = doublet of doublets.

Mass spectrometry. Mass spectrometric measurements were performed by the analytical service of the Institute for Organic Chemistry at the University of Stuttgart. High resolution mass spectra were measured using electrospray ionization (ESI) on a Bruker Daltonics micrOTOF-Q or electron impact (EI) on a Finnigan Mat MAT 95. MS values are given as m/z.

X-ray diffraction. Single-crystal X-ray diffraction analyses were carried out at 100 K on a Bruker Kappa APEXII Duo diffractometer with graphite-monochromated Mo K$_\alpha$ (λ = 0.71073 Å) or Cu K$_\alpha$ (λ = 1.54178 Å) radiaton by using Omega-Phi scan technique.[2] The structures were solved by direct methods using SHELXL97 software. ORTEP molecular graphics were performed by XP software.[3] Crystal structures data were deposited at the Cambridge Crystallographic Data Centre with the respective deposition numbers CCDC 1864076 (**2**) and CCDC 1864077 (**2'**).

Steady-state absorption spectroscopy. Steady-state UV/vis absorption spectra of **1** and **2** were recorded with an Analytik Jena Specord 50 spectrophotometer and of **1'** and **2'** with a JASCO V-670 spectrophotometer. The complexes were dissolved in acetonitrile of spectroscopic grade and measured in a standard 10 mm fluorescence quartz glass cuvette.

Cyclic voltammetry of **1** and **2** was carried out in acetonitrile with 0.1 M Bu$_4$NPF$_6$ as the supporting electrolyte. Complex **2'** was measured in DMF, due to solubility issues. The measurements were performed with an Autolab potentiostat PGSTAT204 from Metrohm using a three-electrode configuration. As working electrode, a glassy carbon disc with a 3 mm diameter stick was used. The counter electrode was a Pt electrode. As reference electrode a non-aqueous Ag/Ag$^+$ electrode (0.01 M AgNO$_3$ in acetonitrile) was utilized with the ferrocene/ferrocenium (Fc/Fc+) couple as reference, added to the solution after each measurement. Thus, all reported potentials are *versus* the Fc/Fc$^+$ couple. All scan rates are 0.1 V/s unless otherwise noted.

DFT calculations. Simulations at the density functional theory (DFT) level were performed using the ORCA program package (Version 4.0.1.2).[4] All calculations used triple zeta valance plus polarization functions (def2-TZVP) basis sets.[5] In order to speed up the calculations, the resolution of identity approximation (RI)

1   H. E. Gottlieb, V. Kotlyar and A. Nudelman, *J. Org. Chem.*, 1997**, 62***, 7512-7515.

2   Bruker, APEX2 and SAINT. Bruker AXs Inc., Madison, Wisconsin, USA, 2008.

3   G. M. Sheldrick, *Acta Cryst*., 2008, **A64**, 112-122.

4   a) F. Neese, *WIREs Comput. Mol. Sci.,* 2017, **8** b) F. Neese, *Interdiscip. Rev. Comput. Mol. Sci.,* 2012, **2,** 73-78.

5   F. Weigend and R. Ahlrichs, *Phys. Chem. Chem. Phys.,* 2005, **7**, 3297-3305.

with a suitable optimized auxiliary basis set was used.[6] The SCF cycles in geometry optimizations and TD-DFT calculations were iterated up to the point where the energy changed by less than 1E-8 atomic units. To ensure converged ground-state geometries, a convergence criterion for the maximum change in energy of at least 1E-8 atomic units and a maximum gradient of at least 1E-4 with a maximal RMS gradient of 1E-6 was chosen. All stationary points on the potential energy surface of the S_0 state were verified by calculations of the energy second derivatives with respect to nuclear coordinates. Geometry optimizations were performed in the gas phase and carried out in redundant internal coordinates. For geometry optimizations of the electronic ground state the BP86 exchange-correlation functional were used.[8] Excited state calculations were carried out with the CAM-B3-LYP functional, starting from ground state structures optimized with the BP86 functional[7]. To account for dispersion effects, the DFTD3 V3.1 correction (D3) by S. Grimme including the Becke-Johnson (BJ) damping is used throughout all calculations.[8] For the calculation of excited states at the time-dependent density functional theory level, the Tamm-Dancoff approximation (tda-TD-DFT) was used. Visualizations of CAM-B3-LYP molecular orbitals were made with carried out with VMD[9] or Mercury 3.9.

Nanosecond transient absorption spectroscopy were performed using a Q-switched pulsed Nd:YAG laser (Q-smart 450mJ, Quantel laser) with pulse durations of approx. 6 ns at a repetition rate of 10 Hz. As excitation pulses the Nd:YAG output centered at 355 nm were used. Afterwards, the excitation light additionally passed a laser line filter (CWL = 355 ± 2 nm, FWHM = 10 ± 2 nm) to ensure that the samples were only excited by 355 nm. The power of the pump beam was about 2 µJ per pulse at the sample, unless otherwise noted. The absorption changes of the samples were probed over the spectral range from 420 nm to 720 nm. To prevent potential damage of the samples by UV light a 400 nm longpass filter were used. The pump and probe beams spatially overlapped at the sample position in a perpendicular beam setup. (Edinburg Instruments, LP980-K spectrometer). The probe lamp was operated in flash mode (150 W ozone-free xenon arc lamp, 40 A). After passing the sample, the probe light was recorded using a photo multiplier tube (Hamamatsu R928P). A standard fused silica cuvette with a layer thickness of 10 mm and a sample OD of approximately 0.4 at the pump wavelength of 355 nm was used in this setup. The compounds **1**, **1'** and **2**, **2'** were dissolved in acetonitrile of spectroscopic grade under inert conditions using an argon filled glovebox.

Photocatalytic measurements. Photocatalytic hydrogen evolution experiments were performed under argon atmosphere with freshly distilled solvents. A double-walled, thermally-controlled reaction vessel was connected to an automatic gas burette and repeatedly evacuated and filled with argon before the copper photosensitizer (ca. 3.5 µmol) and the water reduction catalyst ([Fe$_3$(CO)$_{12}$], ca. 5.0 µmol) were introduced. Subsequently, the solvent mixture (10 mL), composed of THF/TEA/H$_2$O in a volumetric composition of 4/3/1, was added. The temperature of the whole system was maintained at 25 °C by a thermostat. After stirring for at least 5 min at 300 rounds per minute to reach thermal equilibrium, the reaction was started by switching on a Xe lamp (1.5 W output, LOT Quantum Design, without filter). The amount of evolved gases was continuously monitored by the automatic gas burette, while the gas composition was analyzed

[6]   a) K. Eichkorn, O. Treutler, H. Öhm, M. Häser and R. Ahlrichs, *Chem. Phys. Lett.*, 1995, **242**, 652-660 b) F. Weigend, *Phys. Chem. Chem. Phys.*, 2006, **8**, 1057-1065.

[7]   O. Treutler and R. Ahlrichs, *J. Chem. Phys.*, 1995, **102**, 346-354.

[8]   a) S. Grimme, J. Antony, S. Ehrlich and H. Krieg, *J. Chem. Phys.*, 2010, **132**, 154104 b) S. Grimme, S. Ehrlich and L. Goerigk, *J. Comput. Chem.*, 2011, **32**, 1456-1465.

[9]   W. Humphrey, A. Dalke and K. Schulten, *J. Molec. Graphics*, 1996, **14**, 33-38.

by gas chromatography. The photocatalytic experiments have been at least performed twice. The steep slope of the curves at the beginning of the reaction is caused by a temperature rise upon irradiation with the Xenon lamp. A more detailed description of the experimental setup and the applied procedure has been published previously.[10,11]

10   F. Gärtner, S. Losse, A. Boddien, M.-M. Pohl, S. Denurra, H. Junge and M. Beller, *ChemSusChem*, 2012, **5**, 530-533.

11   F. Gärtner, B. Sundararaju, A.-E. Surkus, A. Boddien, B. Loges, H. Junge, P. H. Dixneuf and M. Beller, *Angew. Chem*., 2009, **121**, 10147-10150.

2 Synthetic Details

All chemicals were purchased from commercial suppliers (e.g. Sigma-Aldrich, VWR, Acros Organics or ABCR) and, unless otherwise noted, used as received. Solvents were purified and dried according to standard procedures or directly taken from a Braun solvent purification system.[12] Unless otherwise stated, all reactions which are sensitive towards air or moisture were carried out under dry argon by using standard Schlenk techniques.

1,10-Phenanthroline-5,6-dione and 2,9-dimethyl-1,10-phenanthroline-5,6-dione were synthesized according to previously published literature procedures and matched all reported characterization.[13,14,15]

2.1 Synthesis of the Ligands

Dipyrido[3,2-a:2',3'-c]anthracen-9,10-dinitrile (dpan(CN)$_2$) - L1
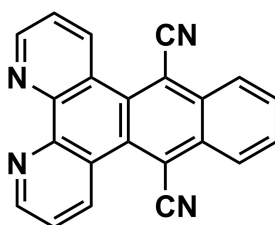
1,10-Phenanthroline-5,6-dione (4.28 mmol, 0.90 g) and 1,2-bis(cyanomethyl)benzene (4.71 mmol, 0.74 g, 1.1 equiv.) were dissolved in acetonitrile (30 mL). After 10 minutes of stirring at ambient temperature DBU (1,8-Diazabicyclo[5.4.0]undec-7-ene, 5.14 mmol, 0.77 mL, 1.2 equiv.) was added dropwise leading to a swift color change. The dark green mixture was then heated to reflux for 2 h. After cooling to room temperature, the resulting yellow precipitate was collected, washed with acetonitrile and dried *in vacuo*.

Yield: 70 % (3.0 mmol, 988 mg).

^{1}H NMR (400 MHz, Chloroform-*d*) δ [ppm]: 9.84 (dd, *J* = 8.5, 1.5 Hz, 2H), 9.23 (dd, *J* = 4.4, 1.5 Hz, 2H), 8.74 – 8.62 (m, 2H), 8.08 – 7.92 (m, 2H), 7.76 (dd, *J* = 8.5, 4.4 Hz, 2H).

**(+)-EI-MS** m/z: [M]$^+$ calculated for C$_{22}$H$_{10}$N$_4$: 330.09; found: 330.09.

---

12 L. A. Wilfred and L. L. C. Christina, *Purification of Laboratory Chemicals* (Sixth Edition), Butterworth-Heinemann, Oxford, 2009.

13 N. Margiotta, V. Bertolasi, F. Capitelli, L. Maresca, A. G. G. Moliterni, F. Vizza and G. Natile, *Inorg. Chim. Acta,* 2004, **357**, 149-158.

14 R.H. Zheng, H.C. Guo, H.J. Jiang, K.H. Xu, B.B. Liu, W.L. Sun and Z.Q. Shen, *Chin. Chem. Lett.,* 2010, **21**, 1270-1272.

15 M. Heberle, S. Tschierlei, N. Rockstroh, M. Ringenberg, W. Frey, H. Junge, M. Beller, S. Lochbrunner and M. Karnahl, *Chem. Eur. J.*, 2017, **23**, 312-319.

3,6-Dimethyldipyrido[3,2-a:2',3'-c]anthracen-9,10-dinitrile (Me$_2$dpan(CN)$_2$) - L2
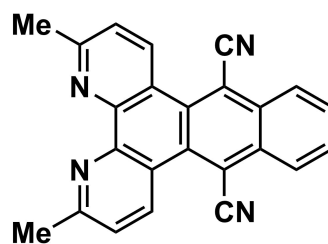
2,9-Dimethyl-1,10-phenanthroline-5,6-dione (1.26 mmol, 300 mg) and 1,2-bis(cyanomethyl)benzene (1.38 mmol, 216 mg, 1.1 equiv.) were dissolved in acetonitrile (20 mL). After 20 minutes of stirring at ambient temperature DBU (1,8-Diazabicyclo[5.4.0]undec-7-ene, 1.51 mmol, 0.23 mL, 1.2 equiv.) was added dropwise and the dark green mixture was then heated to reflux for 1 h. After cooling to room temperature, the resulting pale-yellow precipitate was collected, washed with acetonitrile and dried *in vacuo*.

Yield: 76 % (0.96 mmol, 345 mg).

^{1}H NMR (400 MHz, Chloroform-*d*) δ [ppm]: 9.73 (d, *J* = 8.5 Hz, 2H), 8.73 – 8.63 (m, 2H), 8.06 – 7.89 (m, 2H), 7.63 (dd, *J* = 8.6, 0.4 Hz, 2H), 2.98 (s, 6H).

(+)-EI-MS m/z: [M]$^+$ calculated for C$_{24}$H$_{14}$N$_4$: 358.12; found: 358.12.

2.2   Synthesis of the Cu(I) Complexes

General procedure for the synthesis of homoleptic complexes [Cu(L)$_2$]PF$_6$

[Cu(MeCN)$_4$]PF$_6$ (0.27 mmol, 100 mg, 1 equiv.) and the respective diimine ligand (**L1** or **L2**, 2 equiv.) are suspended in dry and degassed dichloromethane and heated to reflux for 3 h under Ar atmosphere. After cooling to room temperature, the solution is concentrated by rotary evaporation. The complex is then precipitated by adding *n*-hexane. The crude precipitate is filtered, washed thoroughly with water, Et$_2$O and *n*-hexane and dried *in vacuo*.

General procedure for the synthesis of heteroleptic complexes [(xantphos)Cu(L)]PF$_6$

The heteroleptic Cu(I) complexes **1** and **2** were synthesized according to a one-pot two-step procedure following a slightly modified literature protocol.[16,17] In a Schlenk tube, [Cu(MeCN)$_4$]PF$_6$ (0.27 mmol, 100 mg, 1 equiv.) and xantphos (4,5-bis(diphenylphosphino)-9,9-dimethylxanthene, 1 equiv.) are suspended in dry and degassed dichloromethane and heated to reflux for 16 h under Ar atmosphere. After cooling to room temperature, the respective diimine ligand (**L1** or **L2**, 1 equiv.) dissolved in a minimum amount of dichloromethane is added and the reaction is stirred for another 2 h at 30 °C. The protocol for isolation and purification of the final complex is the same as for the homoleptic complexes described above.

[(xantphos)Cu(L1)]PF$_6$ - 1
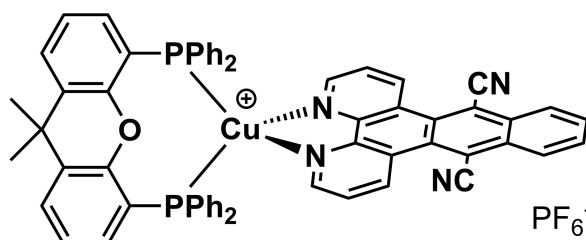
Yield: Yellow solid, 93 % (0.25 mmol, 276 mg).

^{1}H NMR (400 MHz, Acetonitrile-*d*$_3$) δ [ppm]: 9.92 (dd, *J* = 8.6, 1.3 Hz, 1H), 8.77 – 8.67 (m, 1H), 8.60 (dd, *J* = 4.8, 1.3 Hz, 1H), 8.19 – 8.10 (m, 1H), 7.86 – 7.78 (m, 1H), 7.29 – 7.19 (m, 3H), 7.15 – 7.07 (m, 4H), 7.01 (q, *J* = 6.7, 6.0 Hz, 4H), 6.79 – 6.70 (m, 1H), 1.76 (s, 6H).

^{13}C NMR (101 MHz, Acetonitrile-*d*$_3$) δ [ppm]: 155.73, 151.63, 136.84, 135.19, 133.72, 133.64, 133.56, 132.80, 132.06, 131.01, 130.71, 129.78, 129.73, 129.68, 128.99, 127.40, 127.33, 126.48, 126.11, 111.75, 36.95, 28.53, 1.88, 1.67, 1.47, 1.26, 1.05, 0.85, 0.64.

^{31}P NMR (161 MHz, Acetonitrile-*d*$_3$) δ [ppm]: -12.37.

16   S.-P. Luo, E. Mejía, A. Friedrich, A. Pazidis, H. Junge, A.-E. Surkus, R. Jackstell, S. Denurra, Gladiali, S. Lochbrunner and M. Beller, *Angew. Chem.*, 2013, **125**, 437-441.
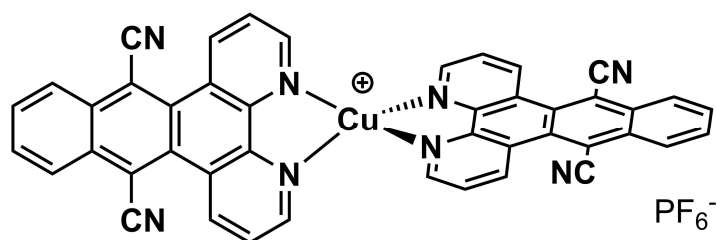
17   E. Mejía, S.-P. Luo, M. Karnahl, A. Friedrich, S. Tschierlei, A.-E. Surkus, H. Junge, S. Gladiali, S. Lochbrunner and M. Beller, *Chem. Eur. J.*, 2013, **19**, 15972-15978.

(+)-ESI-MS (high resolution) **m/z:** [M]$^+$ calculated for $C_{61}H_{42}CuN_4OP_2$: 971.2124; found: 971.2129.

EA for $C_{61}H_{42}CuF_6N_4OP_3$: calculated C = 65.65, H = 3.79, N = 5.01; found C = 64.64, H = 3.83, N = 4.85.

IR $v_{C\equiv N}$ = 2216 cm^{-1}. **UV/vis** λ_{Abs} (ε [10^3 M^{-1}cm^{-1}]): 376 nm (8.3), 394 nm (7.9).

[Cu(L1)₂]PF₆ - 1'

Yield: Dark blackish solid, 73 % (0.20 mmol, 172 mg).

^{1}H NMR (400 MHz, Acetonitrile-d_3) δ [ppm]: 10.14 (s, 1H), 9.03 (s, 1H), 8.74 (s, 1H), 8.16 (dd, J = 6.5, 3.2 Hz, 2H).

^{13}C NMR (101 MHz, Acetonitrile-d_3) δ [ppm]: n.d.

(+)-ESI-MS (high resolution) m/z: [M]$^+$ calculated for $C_{44}H_{20}CuN_8$: 723.1101; found: 723.1107.

EA for $C_{44}H_{20}CuF_6N_8P$ (+CH$_2$Cl$_2$): calculated C = 56.65, H = 2.32, N = 11.74; found: C = 56.32, H = 2.23, N = 11.53.

UV/vis λ_{Abs} (ε [10^3 M^{-1}cm^{-1}]): 377 nm (16.4), 394 nm (15.9), 452 nm (5.7).

[(xantphos)Cu(L2)]PF₆ – 2
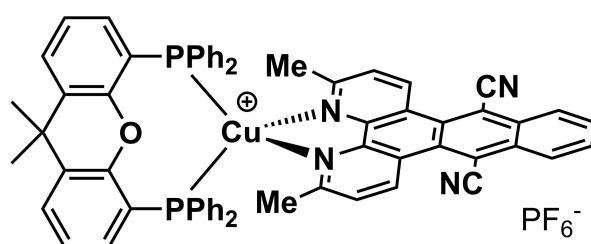
Yield: Orange solid, 90 % (0.24 mmol, 273 mg).

^{1}H NMR (400 MHz, Acetonitrile-d_3) δ [ppm]: 9.69 (d, J = 8.6 Hz, 1H), 8.73 – 8.64 (m, 1H), 8.15 – 8.06 (m, 1H), 7.78 (dd, J = 7.8, 1.4 Hz, 1H), 7.68 (d, J = 8.7 Hz, 1H), 7.30 – 7.18 (m, 3H), 7.18 – 7.02 (m, 9H), 2.31 (s, 3H), 1.73 (s, 3H).

^{13}C NMR (101 MHz, Acetonitrile-d_3) δ [ppm]: 161.52, 145.14, 136.81, 134.72, 133.99, 133.92, 133.84, 133.34, 132.39, 132.24, 132.08, 131.91, 131.22, 131.02, 130.55, 129.69, 129.64, 129.60, 129.06, 127.18,

126.36, 124.77, 122.05, 110.72, 36.81, 32.24, 28.93, 27.62, 23.28, 14.32, 1.88, 1.67, 1.47, 1.26, 1.05, 0.85, 0.64.
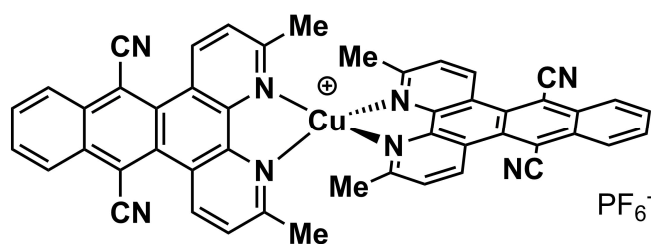
^{31}P NMR (161 MHz, Acetonitrile-d_3) δ [ppm]: -12.44.

(+)-ESI-MS (high resolution) **m/z:** [M]$^+$ calculated for $C_{63}H_{46}CuN_4OP_2$: 999.2437; found: 999.2431.

EA for $C_{63}H_{46}CuF_6N_4OP_3$: calculated C = 66.06, H = 4.05, N = 4.89; found: C = 65.45, H = 4.37, N = 4.62.

IR $v_{C\equiv N}$ = 2218 cm^{-1}. **UV/vis** λ_{Abs} (ε [10^3 M^{-1}cm^{-1}]): 383 nm (11.1), 400 nm (10.5).

[Cu(L2)$_2$]PF$_6$ - 2'

Yield: Brown solid, 76 % (0.20 mmol, 191 mg).

^{1}H NMR (400 MHz, Acetonitrile-d_3) δ [ppm]: 10.03 (d, J = 8.6 Hz, 2H), 8.70 (dd, J = 6.5, 3.2 Hz, 2H), 8.11 (dd, J = 6.5, 3.2 Hz, 2H), 8.01 (d, J = 8.7 Hz, 2H), 2.52 (s, 6H).

^{13}C NMR (101 MHz, Acetonitrile-d_3) δ [ppm]: 161.20, 145.64, 136.42, 133.33, 132.44, 130.93, 127.16, 126.82, 125.12, 111.23, 26.02, 1.88, 1.67, 1.46, 1.26, 1.05, 0.85, 0.64.

 (+)-ESI-MS (high resolution) m/z: [M]$^+$ calculated for $C_{48}H_{28}CuN_8$: 779.1727; found: 779.1746.

EA for $C_{48}H_{28}CuF_6N_8P$ (+CH$_2$Cl$_2$): calculated C = 58.26, H = 2.99, N = 11.09; found: C = 59.89, H = 3.03, N = 11.57.

UV/vis λ_{Abs} (ε [10^3 M^{-1}cm^{-1}]): 380 nm (20.0), 398 nm (19.8), 458 nm (10.8)

3 NMR and MS spectra of the Complexes 1, 1' and 2, 2'
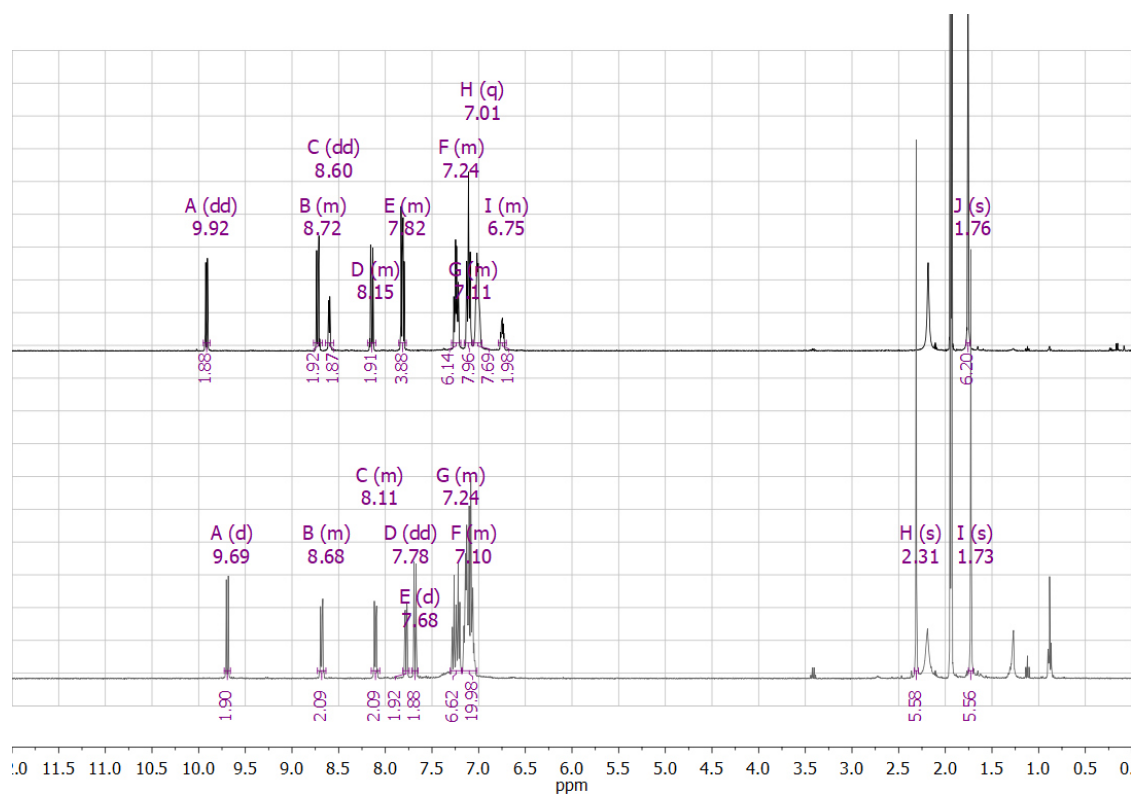
Fig. S1. Presentation of the ¹H-NMR spectra (at 400 MHz, in Acetonitrile-d_3) of the heteroleptic copper complexes **1** (black, top) and **2** (grey, bottom).
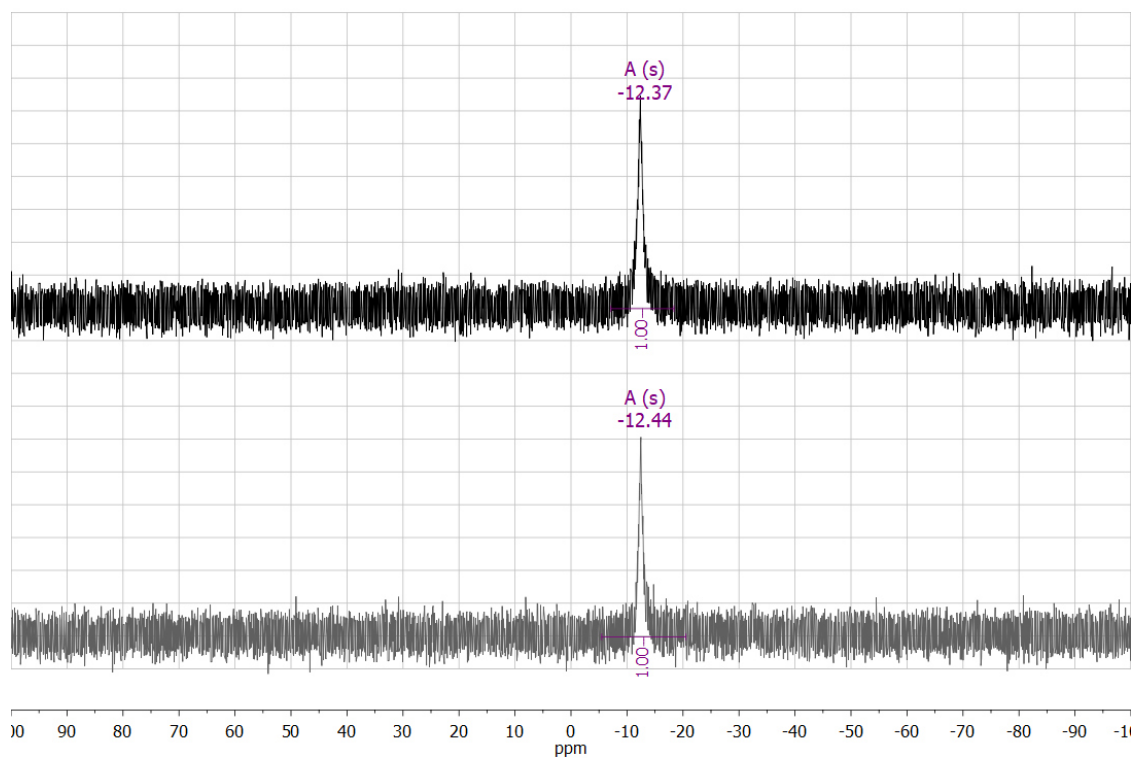

Fig. S2. Comparison of the ³¹P{¹H}-NMR spectra (at 161 MHz, in Acetonitrile-d_3) of the heteroleptic copper complexes **1** (black, top) and **2** (grey, bottom).
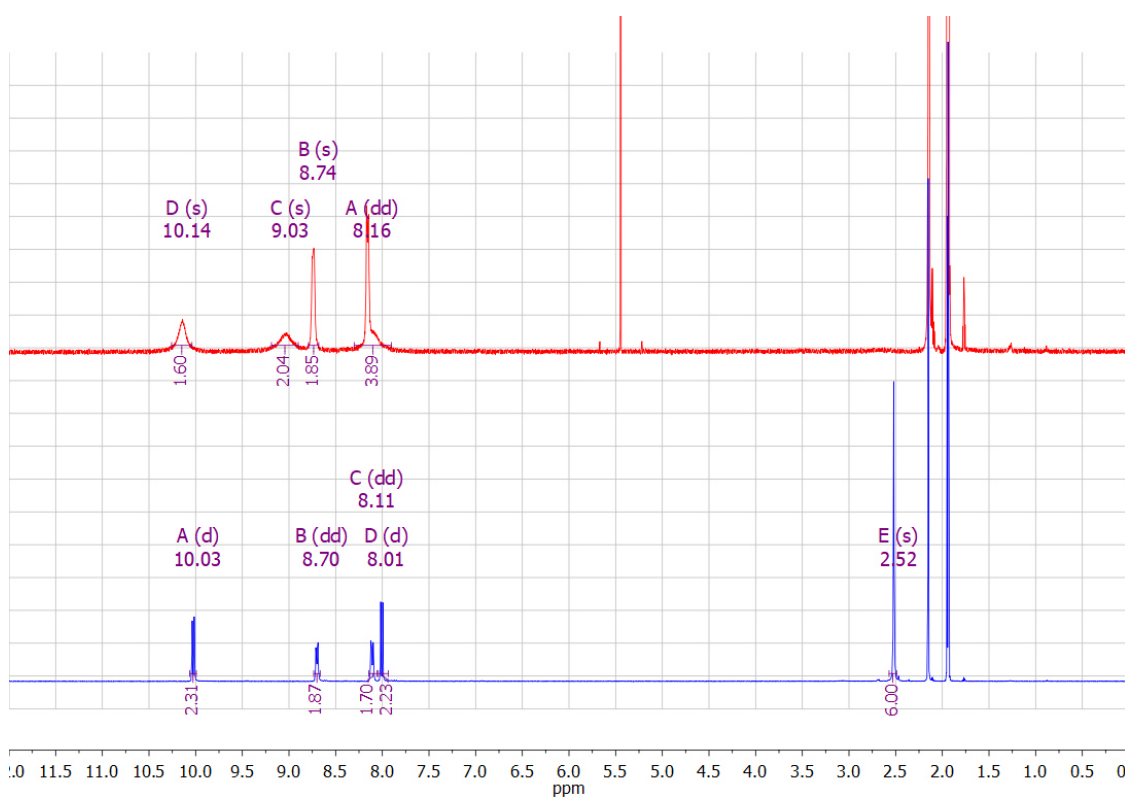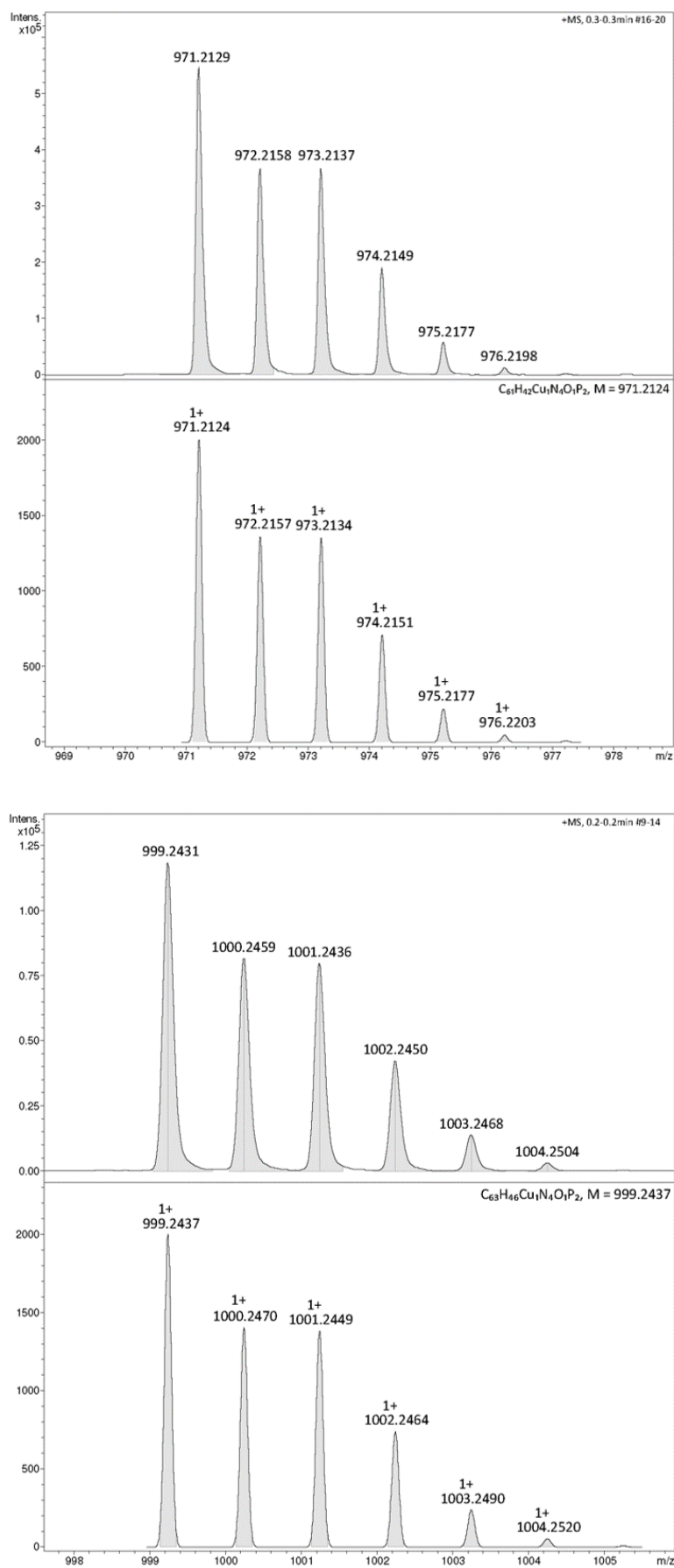
Fig. S3. Presentation of the ^{1}H-NMR spectra (at 400 MHz, in Acetonitrile-d_3) of the homoleptic copper complexes **1'** (red, top) and **2'** (blue, bottom).

Fig. S4. High resolution (+)-ESI mass spectra of the heteroleptic complexes **1** (top) and **2** (bottom) with matching isotopic pattern.
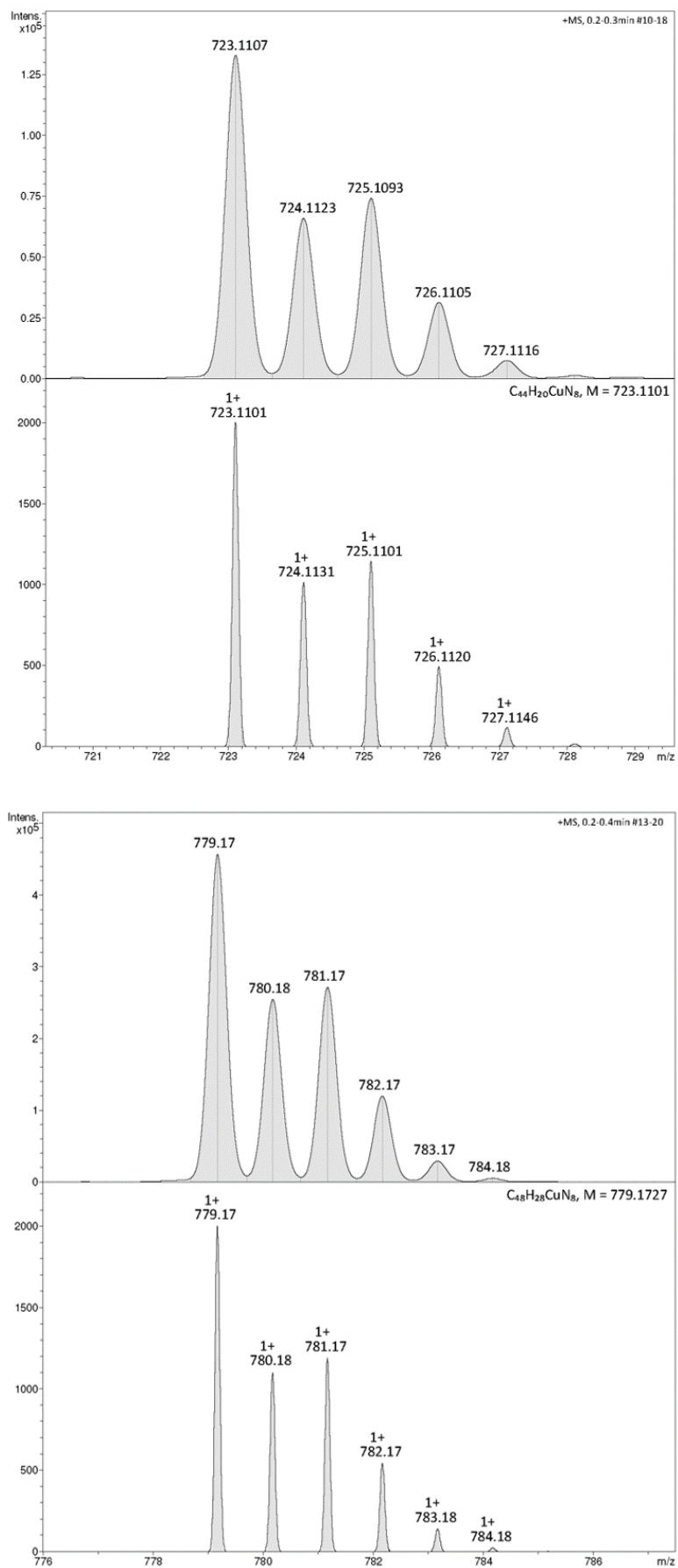
Fig. S5. High resolution (+)-ESI mass spectra of the homoleptic complexes **1'** (top) and **2'** (bottom) with matching isotopic pattern.

4　Crystallographic Data and Structures of the Complexes 2 and 2'

Table S1. Crystallographic data and refinement details of the copper complexes **2** and **2'**.

Compound	2	2'
CCDC number [#]	CCDC 1864076	CCDC 1864077
Empirical formula	$C_{63}H_{46}CuF_6N_4OP_3$	$C_{48}H_{28}CuF_6N_8P$
Formula weight	1145.49	925.29
Temperature (K)	130(2)	130(2)
Wavelength (Å)	0.71073	1.54178
Crystal system, space group	Triclinic, P-1	Triclinic, P -1
Unit cell dimensions (Å, °)		
a	11.2628(9)	8.1362(5)
b	12.4158(9)	10.6863(7)
c	21.9828(19)	22.4625(13)
α	83.055(4)	86.186(4)
β	78.448(4)	81.280(4)
γ	87.667(3)	87.085(5)
Volume (Å^3)	2989.2(4)	1924.5(2)
Z, calculated density (Mg m^{-3})	2, 1.273	2, 1.597
Absorption coefficient (mm^{-1})	0.507	1.876
F(000)	1176	940
Crystal size (mm)	0.309 x 0.168 x 0.164	0.16 x 0.10 x 0.05
Theta range for data collection (°)	1.653 to 26.422	4.15 to 65.59
Limiting indices	-14<=h<=14, -15<=k<=15, -27<=l<=27	-7<=h<=9, -12<=k<=12, -22<=l<=26
Reflections collected / unique	49288 / 12239 [R(int) = 0.0411]	23569 / 6457 [R(int) = 0.0519]
Completeness to theta = 25.242 (65.59)	99.8	96.9
Absorption correction	Semi-empirical from equivalents	Numerical
Max. and min. transmission	0.7454 and 0.7032	0.9210 and 0.7266
Refinement method	Full-matrix least-squares on F^2	Full-matrix least-squares on F^2
Data / restraints / parameters	12239 / 12 / 707	6457 / 0 / 581
Goodness-of-fit on F^2	1.038	1.031
Final *R* indices [*I>2σ(I)*]	R1 = 0.0405, wR2 = 0.0918	R1 = 0.0423, wR2 = 0.1077
R indices (all data)	R1 = 0.0686, wR2 = 0.0984	R1 = 0.0589, wR2 = 0.1159
Largest diff. peak and hole (e.Å^{-3})	0.439 and -0.312	0.398 and -0.351

[#] CCDC 1864076 (**2**) and 1864077 (**2'**) contain the supplementary crystallographic data for this paper. These data are provided free of charge by the Cambridge Crystallographic Data Centre.
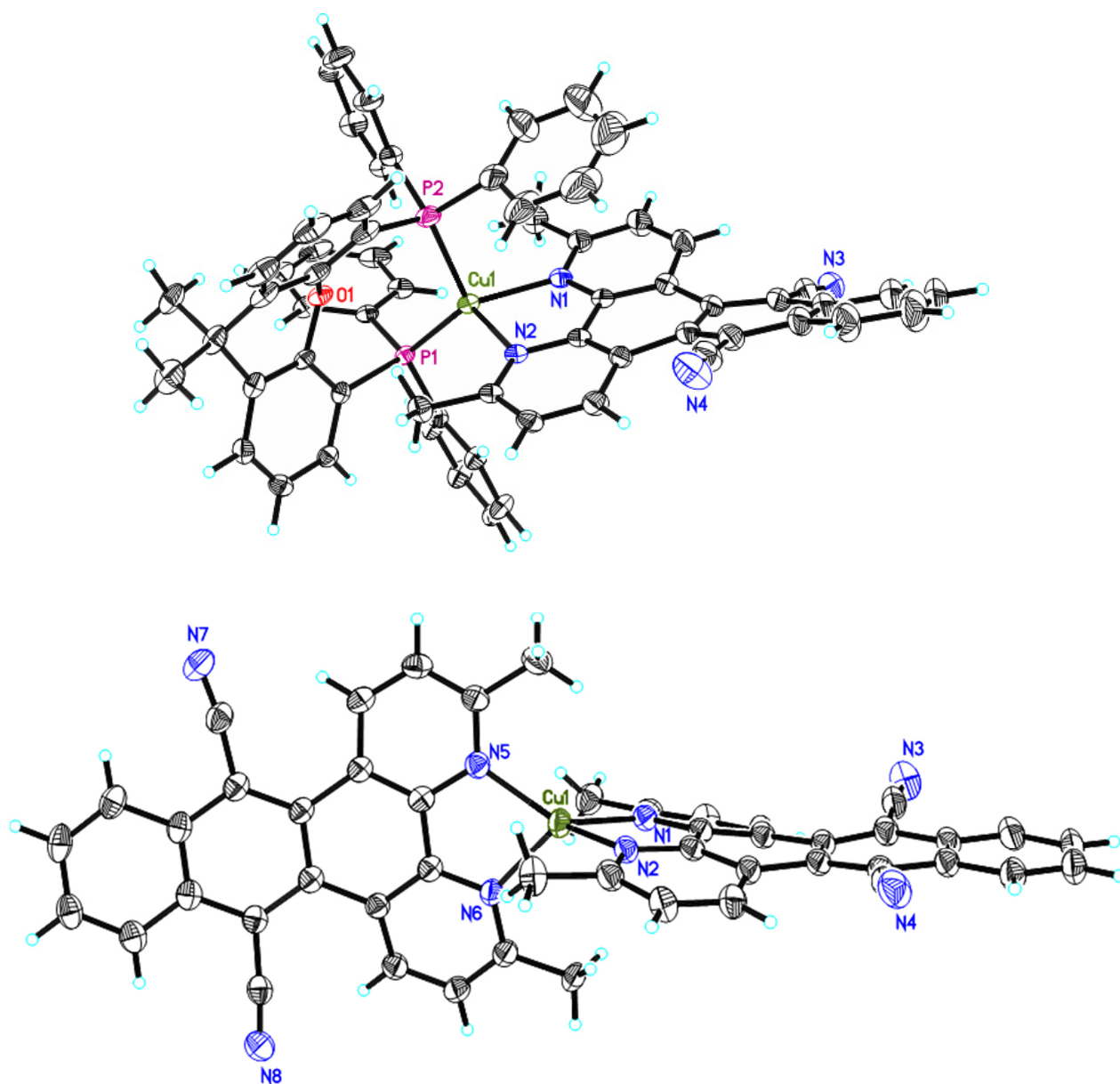
Fig. S6. Comparison of the solid-state structures (ORTEP representation) of complex **2** and **2'** with thermal ellipsoids at a probability level of 50 %. The PF_6^- counter anion is omitted for clarity in both cases. Special attention should be given to the strongly twisted ligand **L2**. In comparison to Fig. 2 in the main text the hydrogen atoms are shown in this visualization and the orientation of the molecule is changed.
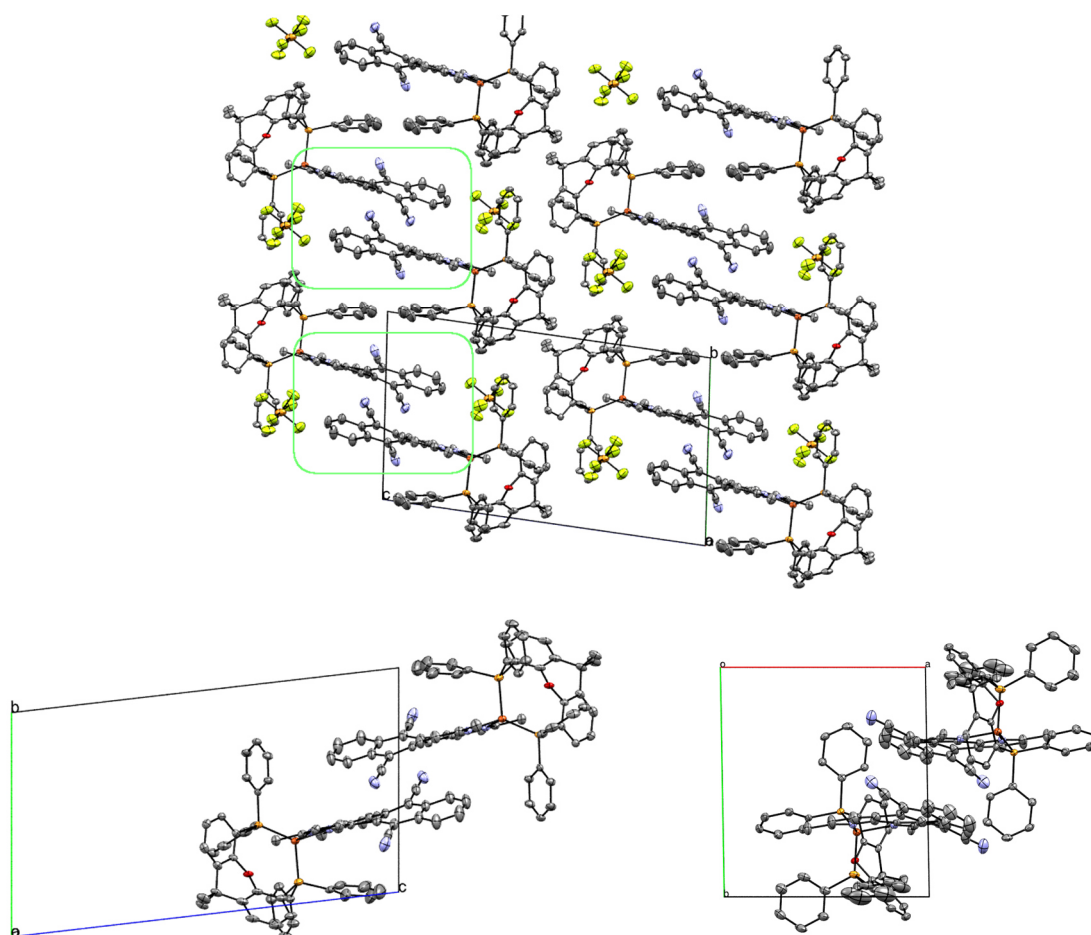
Fig. S7. ORTEP representation of the unit cell of complex **2** with thermal ellipsoids at a probability level of 50 %. The hydrogen atoms are omitted for clarity. In the extended crystal structure, a pairwise stacking of the ligand **L2** between neighboring complexes is found in the solid state (see highlighted area). The bottom pictures show an enlargement of packing situation with view along the a-axis (left) and b-axis (right). The two molecules have an offset along the a-axis, due to the twist of the diimine-ligand.
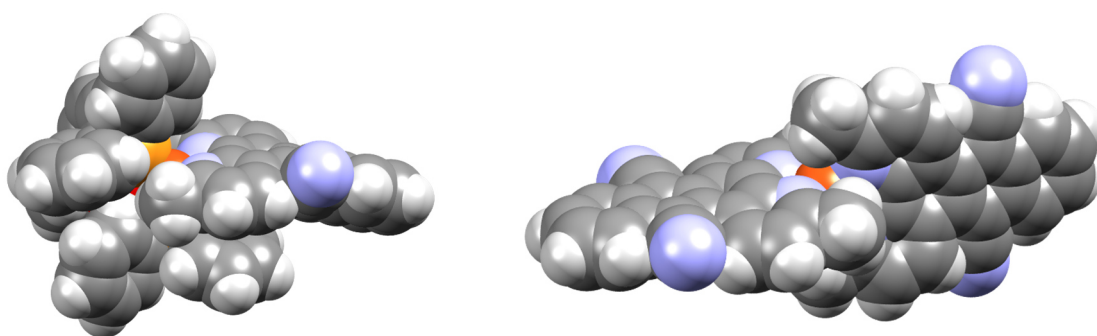
Fig. S8. Solid state structure (space filled representation) of the crystal structure of complex **2** (left) and **2'** (right) (Cu = brown, P = orange, N = blue, O = red, C = gray and H = light gray), illustrating the strong shielding of the copper center by the bulky ligands and the twisting of **L2** due to lack of space caused by the two nitrile substituents.

Table S2. Additional crystallographic bond angles (°) of the copper complexes **2** and **2'**.

	2 heteroleptic		**2'** homoleptic
N1-Cu1-P1	128.17(5)	N1-Cu1-N6	117.58(8)
N1-Cu1-P2	102.73(5)	N1-Cu1-N5	129.18(9)
N2-Cu1-P2	103.73(5)	N2-Cu1-N5	135.92(9)
N2-Cu1-P1	118.97(5)	N2-Cu1-N6	117.12(8)
N1-Cu1-N2	79.12(7)	N1-Cu1-N2	80.47(9)
P1-Cu1-P2	116.69(2)	N5-Cu1-N6	80.63(8)
Twist Ring A/D	12.61	Twist Ring A/D	10.74
Twist Ring D/E	17.00	Twist Ring D/E	5.30
Twist Ring A/E	29.10	Twist Ring A/E	11.38
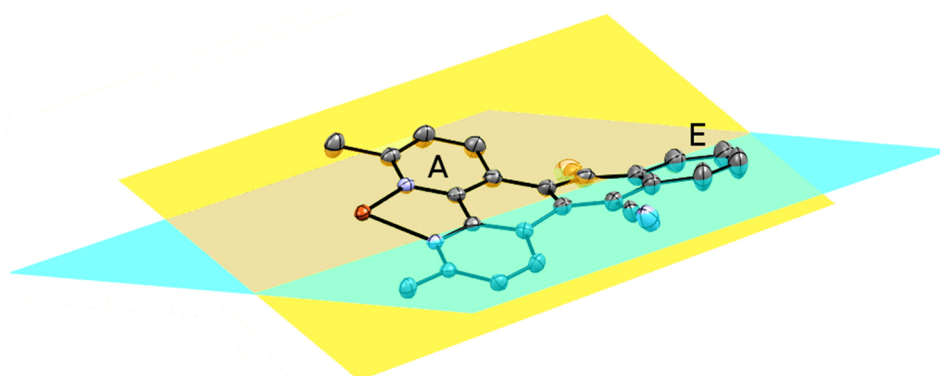
Fig. S9. Another visualization of the distortion of the ligand **L2** in the crystal structure of complex **2**. Calculated planes through ring A (yellow) and ring E (blue) of **L2** (see Table SI2). The xantphos ligand as well as hydrogen atoms are omitted for a better visibility.

5   Calculated Ground State Structures of 1, 1' and 2, 2' and 3
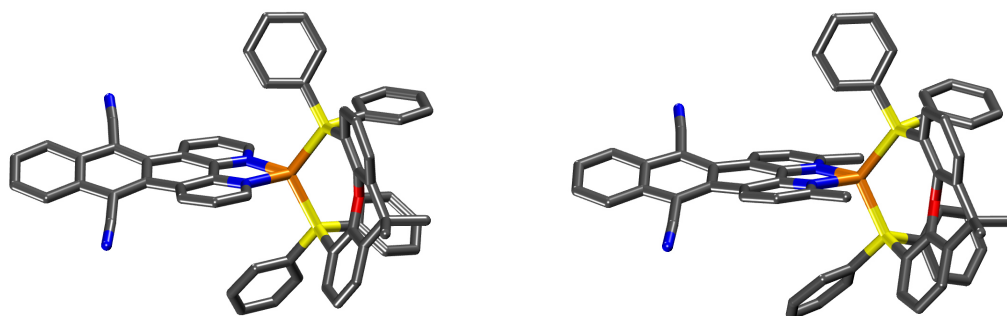
Fig. S10 Calculated ground state structure of the heteroleptic complex **1** (left) and **2** (right) optimized at the BP86-D3(BJ)/def2-TZVP level of theory (Cu = brown, P = orange, N = blue, O = red and C = grey). Hydrogen atoms are omitted for clarity.
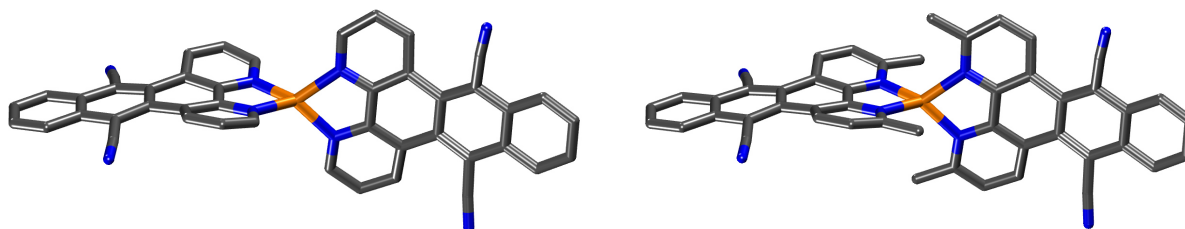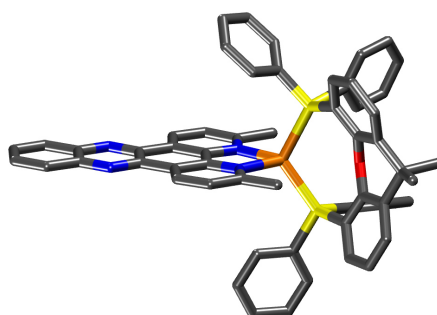

Fig. S11. Calculated ground state structure of the homoleptic complex **1'** (left) and **2'** (right) optimized at the BP86-D3(BJ)/def2-TZVP level of theory (Cu = brown, P = orange, N = blue, O = red and C = grey). Hydrogen atoms are omitted for clarity.

Fig. S12. Calculated ground state structure of complex **3** optimized at the BP86-D3(BJ)/def2-TZVP level of theory for comparison. (Cu = brown, P = orange, N = blue, O = red and C = grey). Hydrogen atoms are omitted for clarity.

6   Steady-state Absorption and Emission Spectra of 1 and 2
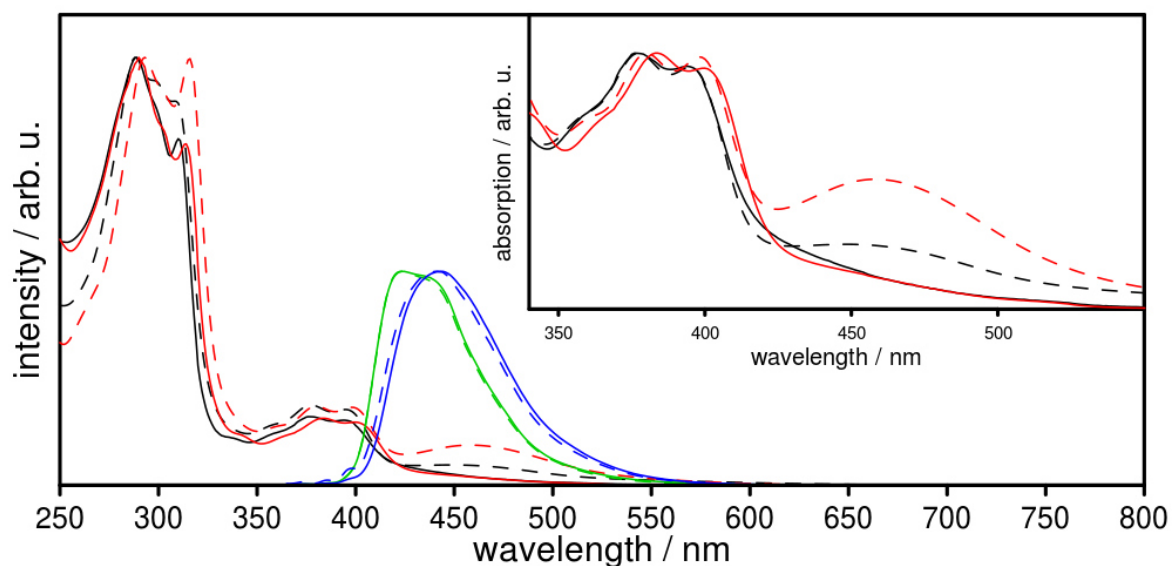
Fig. S13 Normalized UV/vis absorption of **1** (black, solid), **1'** (black, dashed), **2** (red, solid), **2'** (red, dashed) and and emission spectra of **1** (green, solid), **1'** (green, dashed), **2** (blue, solid), **2'** (blue, dashed) in acetonitrile under inert conditions. The inset represents an enlargement of the UV/vis spectra in the range of the metal-to-ligand charge transfer transition. The emission (plotted in the middle) was recorded after excitation at 355 nm and can clearly be assigned to originate from uncoordinated ligand **L1** or **L2**, respectively (not explicitely shown).
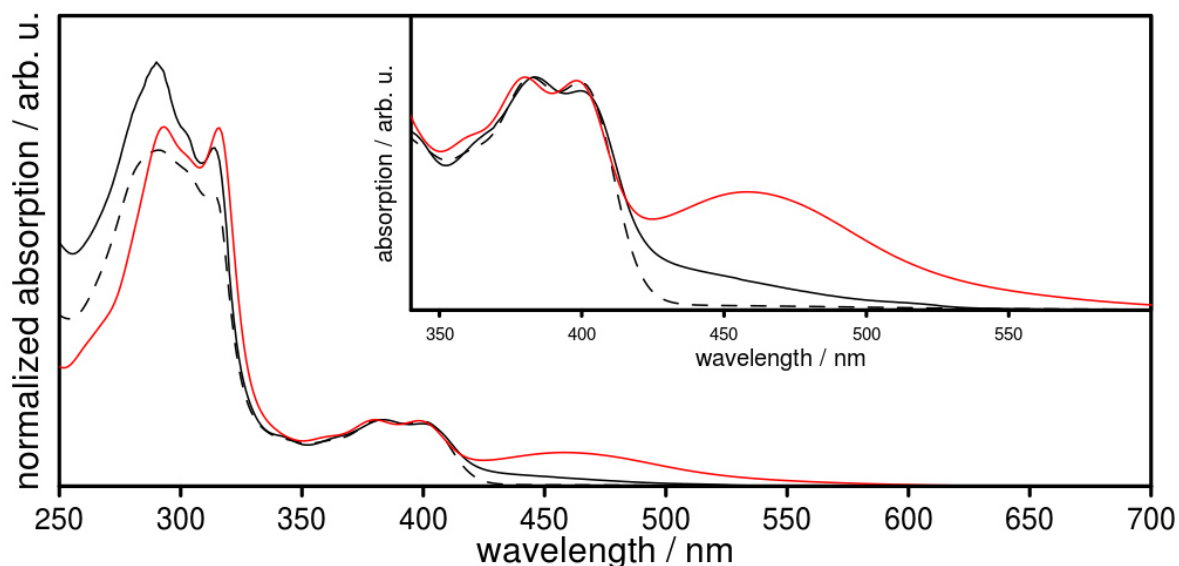
Fig. S14 Normalized UV/vis absorption spectra of **2** (black, solid), **L2** (black, dashed) and **2'** (red, solid) in acetonitrile under inert conditions. The inset represents an enlargement of the UV/vis spectra in the range of the metal-to-ligand charge transfer and the lowest lying π-π* transitions. The maxima (in descending order) occur at 400, 383, 314, 290 nm for **2**, 458, 398, 380, 316, 293 nm for **2'**, and at 399, 382, 314, 291 nm for **L2**.
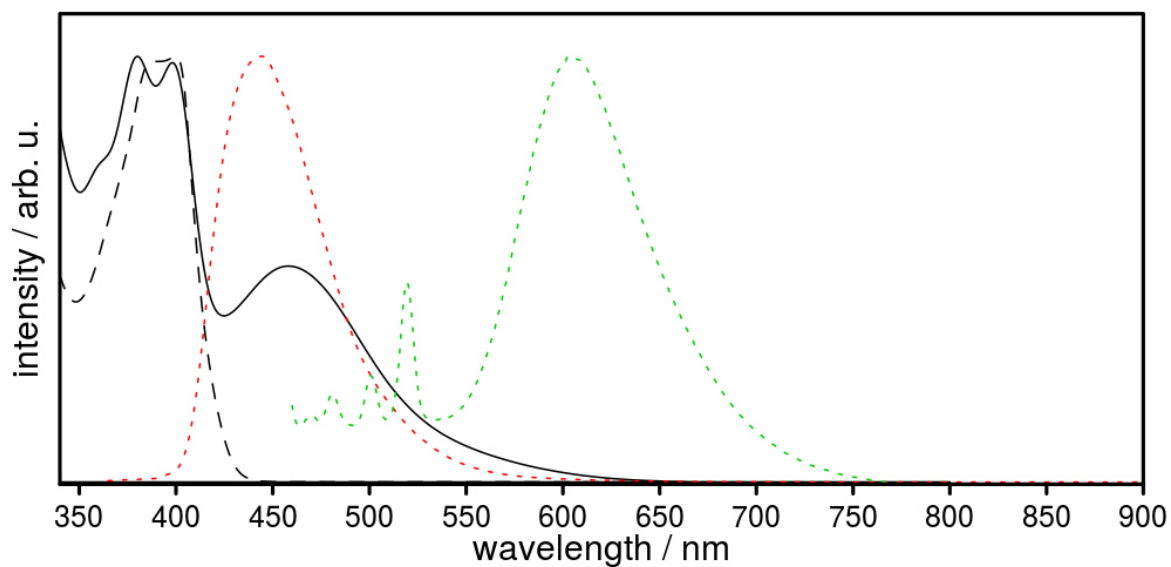
Fig. S15 Normalized UV/vis absorption spectra of **2** (black, solid), **L2** (black, dashed) and normalized emission spectra of **2** after excitation at 355 nm (red, dotted) and after exciatation at 450 nm (green, dotted). The measurements were performed in acetonitrile under inert conditions. The emission maximum after excitation at λ = 355 nm occurs at 444 nm and is the same as for the uncoordinated ligand **L2**. The very weak emission after excitation at λ = 450 nm has its maximum at 605 nm.

7 TD-DFT Calculations of the Absorption Spectra of 1 and 2
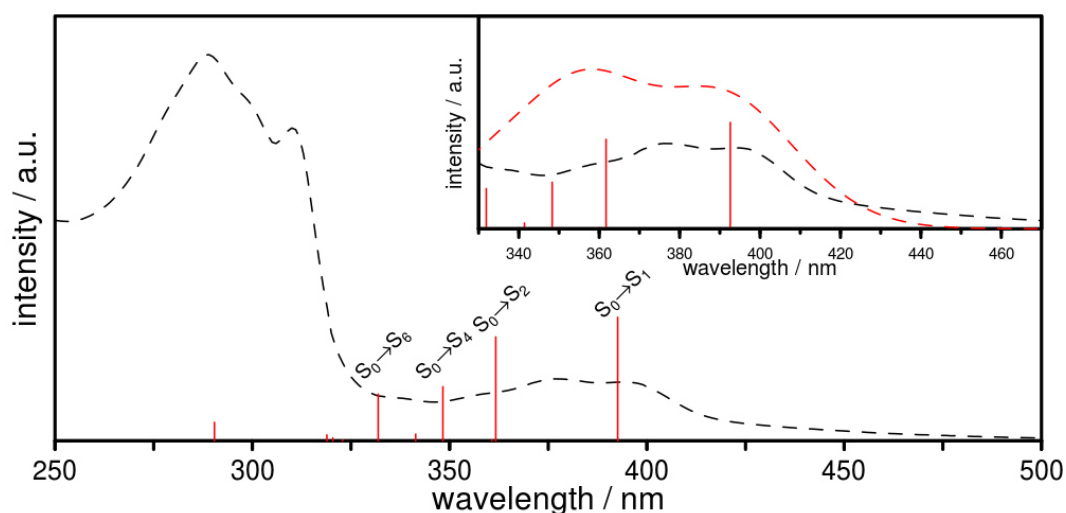
Fig. S16. Measured UV/vis absorption spectrum of complex **1** in acetonitrile (black, dashed) and calculated lowest-lying singlet excitation energies (red vertical lines). The inset represents an enlargement of the MLCT region with a simulated spectrum (red, dashed) as summation of gaussians centered at each excitation energy and weighted with their respective oscillator strength. Please note, that only the first 10 singlet transitions have been calculated.

Table S3. Calculated excitation energies and transition moments of complex **1** at TD-DFT level (CAM-B3LYP-D3(BJ)/def2-TZVP) with CPCM (acetonitrile) solvation model. Only excitation with an oscillator strength > 0.01 and corresponding orbital contributions with $|coeff.|^2$ *100 > 0.09 are listed. Compare with the differential densities in Fig. S18 and the orbital pictures in Fig. S19. The description "ant" refers to the central anthracene moiety of the ligand, whereas "dcb" refers to the dicyanobenzol part of the ligand and "phen" to the phenanthroline part (see also Fig. S17).

| State	Excitation energy		Oscillator	Dominant contributions			Transitions
#	cm^{-1}	nm	strength	occ. orb.	virt. Orb.	$|coeff.|^2$*100	
1	25470.2	392.6	0.12965036	HOMO	LUMO	0.66429	$Cu_d \rightarrow \pi_{dcb}, \pi_{ant}$
2	27650.5	361.7	0.10902437	HOMO	LUMO+1	0.226479	$Cu_d \rightarrow \pi_{phen}$
4	28712.8	348.3	0.05676872	HOMO-3	LUMO	0.880104	$\pi_{ant}, \pi_{dcb} \rightarrow \pi_{dcb}, \pi_{ant}$
				HOMO	LUMO	0.162778	$Cu_d \rightarrow \pi_{dcb}, \pi_{ant}$
				HOMO	LUMO+1	0.643093	$Cu_d \rightarrow \pi_{phen}$
6	30133.8	331.9	0.04900533	HOMO-10	LUMO	0.28066	$\pi_{ant} \rightarrow \pi_{dcb}, \pi_{ant}$
				HOMO-3	LUMO+2	0.271665	$\pi_{ant}, \pi_{dcb} \rightarrow \pi_{phen}, \pi_{ant}$
				HOMO	LUMO	0.101055	$Cu_d \rightarrow \pi_{dcb}, \pi_{ant}$
10	34437.2	290.4	0.01937822	HOMO-4	LUMO+2	0.458418	$Cu_d \rightarrow \pi_{phen}, \pi_{ant}$
				HOMO-3	LUMO+1	0.302347	$\pi_{ant}, \pi_{dcb} \rightarrow \pi_{phen}$
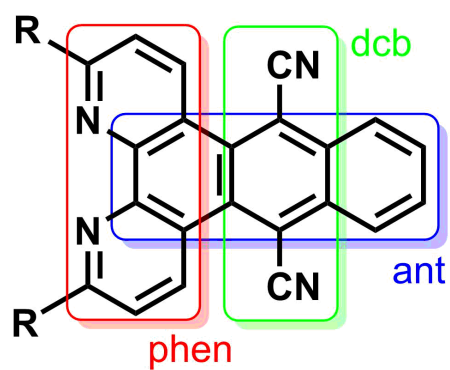
Fig. S17. Illustration of the abbreviations applied in the Tables S3 and S4 used for the categorization of the calculated UV/vis excitations. The description "ant" refers to the central anthracene moiety of the ligand, whereas "dcb" refers to the dicyanobenzol part of the ligand and "phen" to the phenanthroline part.
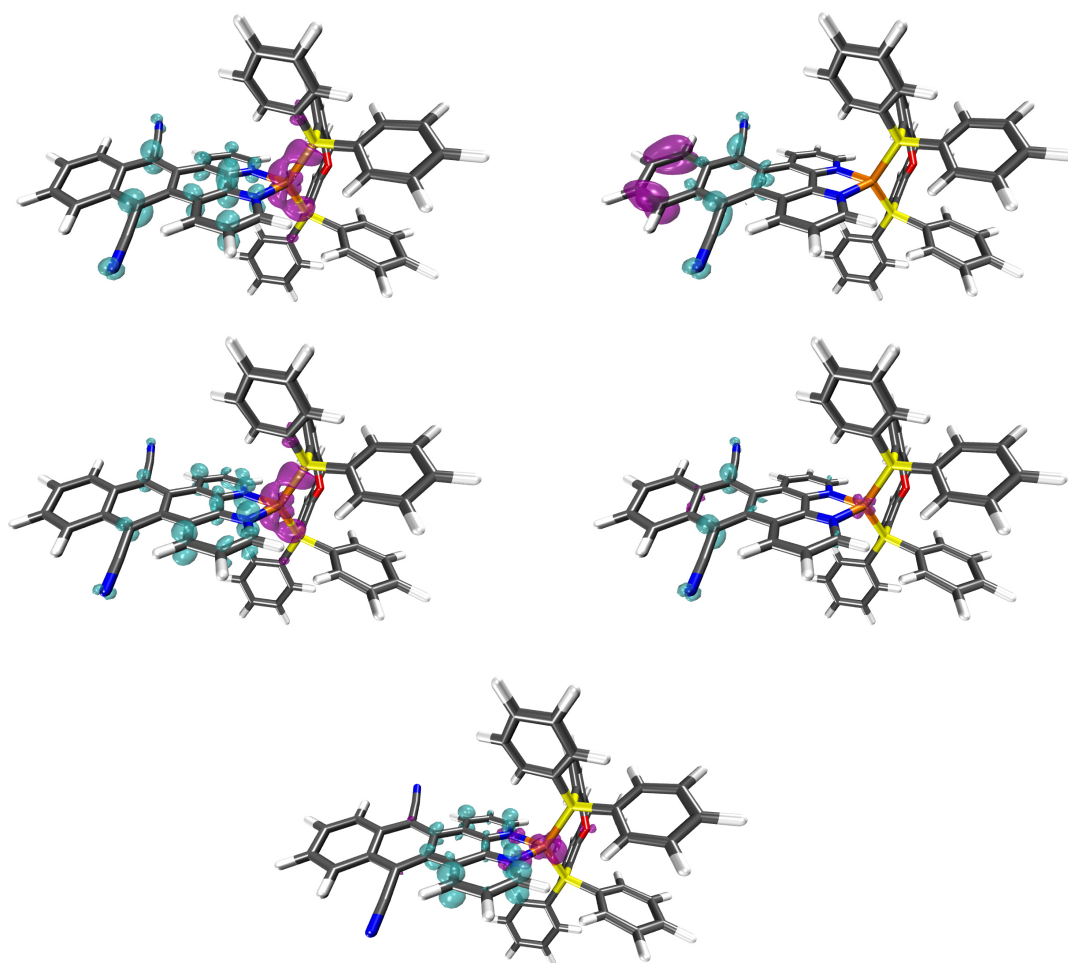
Fig. S18. Differential density plots of **1** between the ground state and the singlet excited states 1 (top left), the singlet excited state 2 (top right), singlet excited state 4 (middle left), singlet excited state 6 (middle right), and singlet excited state 10 (bottom), respectively. Cyan corresponds to a positive isovalue in the density difference between the single-electron matrices of the ground and excited state. Purple corresponds to a negative isovalue, and hence, a decline in electron density. Compare also with Fig. S19 and Table S3.
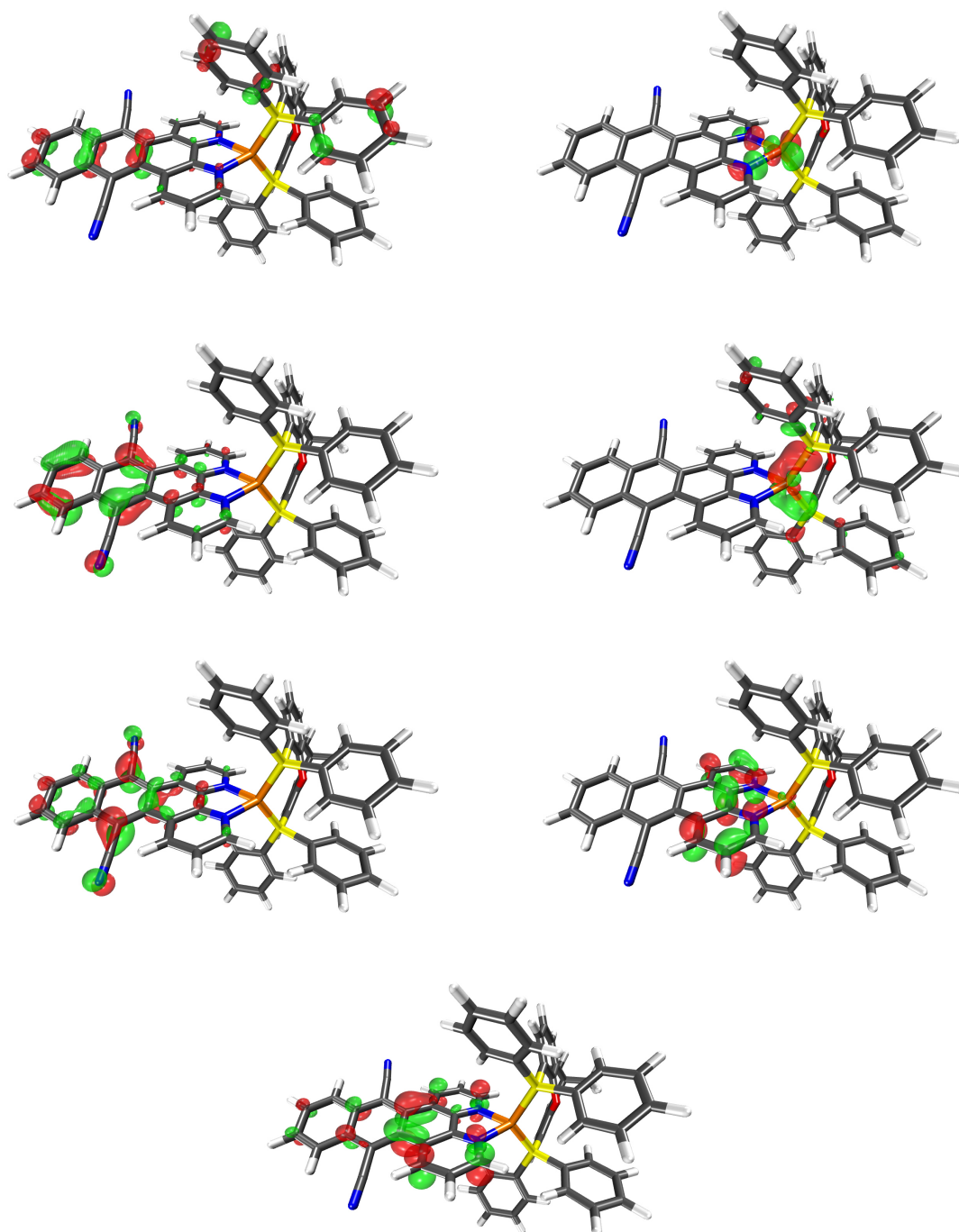
Fig. S19. Presentation of the HOMO-10 (top left), HOMO-4 (top right), HOMO-3 (2nd row left), HOMO (2nd row right), LUMO (3rd row left), LUMO+1 (3rd row right) and LUMO+2 (bottom) orbitals of complex **1** at CAM-B3LYP-D3(BJ)/CPCM(acetonitrile)/def2-TZVP level of theory.

Table S4. Calculated excitation energies and transition moments of complex **2** at tda TD-DFT level (CAM-B3LYP-D3(BJ)/def2-TZVP) with CPCM (acetonitrile) solvation model. Only excitation with an oscillator strength > 0.01 and corresponding orbital contributions with $|coeff.|^2 *100 > 0.09$ are listed. Compare with the differential densities in Fig. S20 and the orbital pictures in Fig. S21. The description "ant" refers to the central anthracene moiety of the ligand, whereas "dcb" refers to the dicyanobenzol part of the ligand and "phen" to the phenanthroline part (see also Fig. S17).

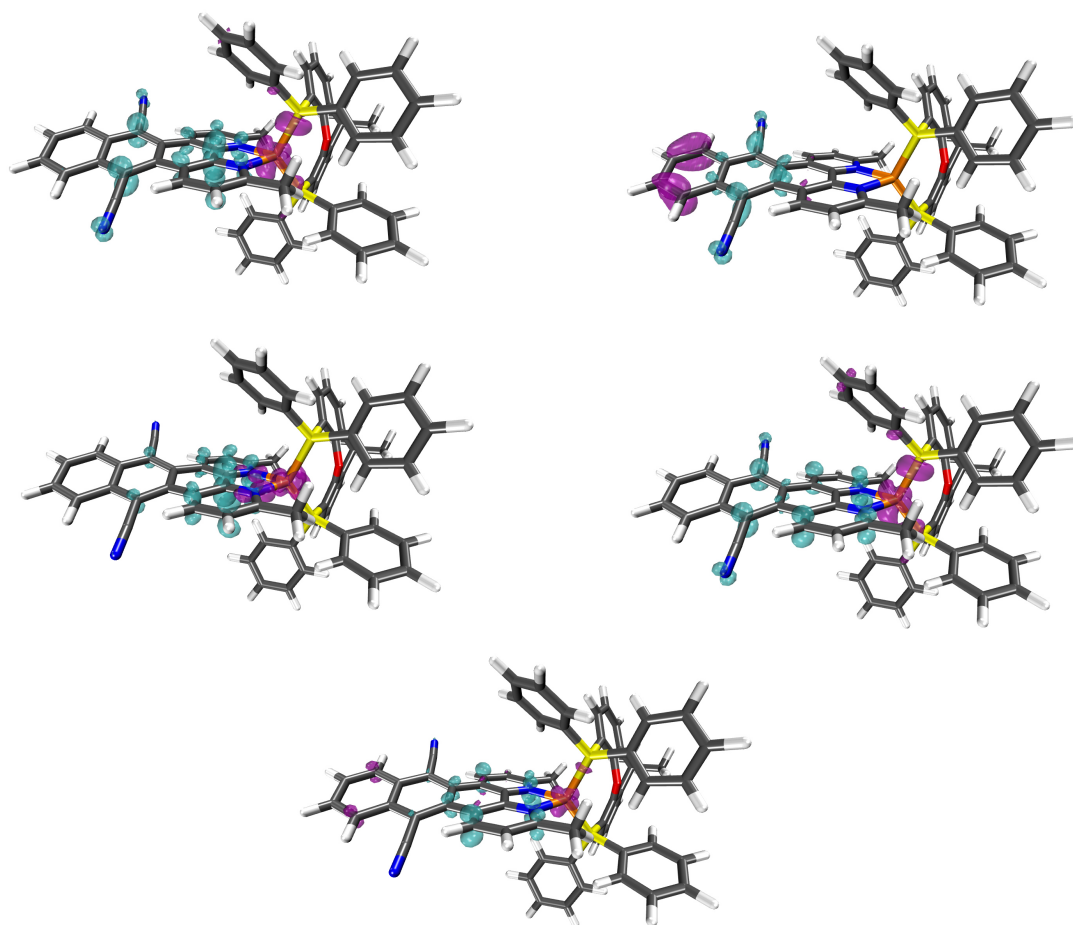| State	Excitation energy		Oscillator	Dominant contributions			Transitions
#	cm^{-1}	nm	strength	occ. orb.	virt. Orb.	$|coeff.|^2*100$	
1	26563.0	376.5	0.14559625	HOMO	LUMO	0.61474	$Cu_d \rightarrow \pi_{dcb}, \pi_{ant}$
2	27542.5	363.1	0.11358278	HOMO	LUMO+1	0.207059	$Cu_d \rightarrow \pi_{phen}$
3	28860.2	346.5	0.01264544	HOMO-1	LUMO	0.852871	$\pi_{ant}, \pi_{dcb} (,\pi_{phen}) \rightarrow \pi_{dcb}, \pi_{ant}$
				HOMO-4	LUMO	0.18491	$Cu_d \rightarrow \pi_{dcb}, \pi_{ant}$
				HOMO-4	LUMO+1	0.572054	$Cu_d \rightarrow \pi_{phen}$
5	30208.4	331.0	0.05248955	HOMO	LUMO	0.287106	$Cu_d \rightarrow \pi_{dcb}, \pi_{ant}$
				HOMO	LUMO+1	0.429428	$Cu_d \rightarrow \pi_{phen}$
10	34563.0	289.3	0.06058115	HOMO-15	LUMO	0.212045	$\pi_{phen}, \pi_{ant}, Cu_d \rightarrow \pi_{dcb}, \pi_{ant}$
				HOMO-1	LUMO+1	0.2918	$\pi_{ant}, \pi_{dcb} (,\pi_{phen}) \rightarrow \pi_{phen}$
				HOMO	LUMO+2	0.268806	$Cu_d \rightarrow \pi_{ant}, \pi_{phen}$

Fig. S20. Differential density plots of **2** between the ground state and the singlet excited states 1 (top left), the singlet excited state 2 (top right), singlet excited state 3 (middle left), singlet excited state 5 (middle right), and singlet excited state 10 (bottom), respectively. Cyan corresponds to a positive isovalue in the density difference between the single-electron matrices of the ground and excited state. Purple corresponds to a negative isovalue, and hence, a decline in electron density. Compare also with Fig. S21 and Table S4.
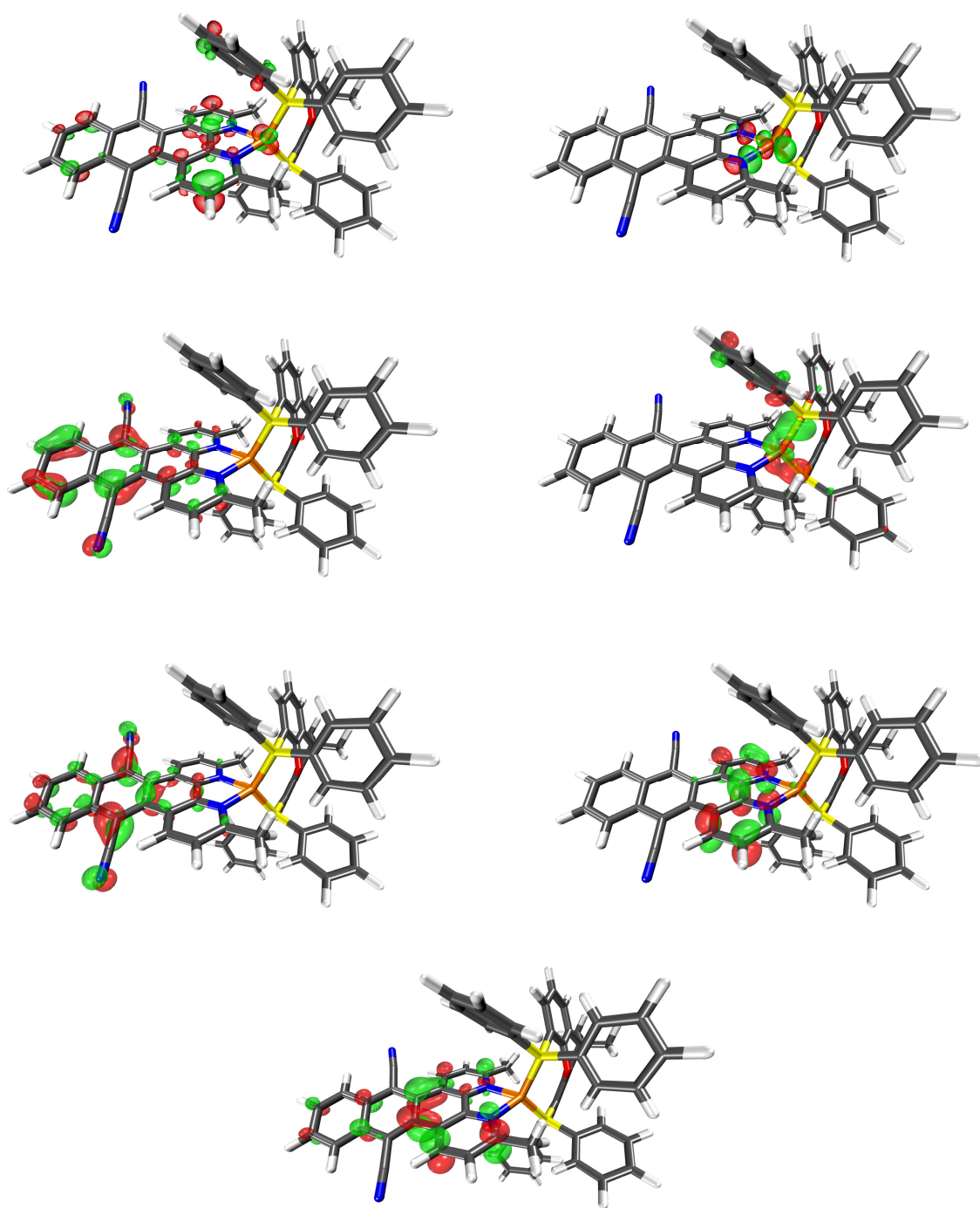
Fig. S21. Presentation of the HOMO-15 (top left), HOMO-4 (top right), HOMO-1 (2nd row left), HOMO (2nd row right), LUMO (3rd row left), LUMO+1 (3rd row right) and LUMO+2 (bottom) orbitals of complex **2** at CAM-B3LYP-D3(BJ)/CPCM(acetonitrile)/def2-TZVP level of theory.
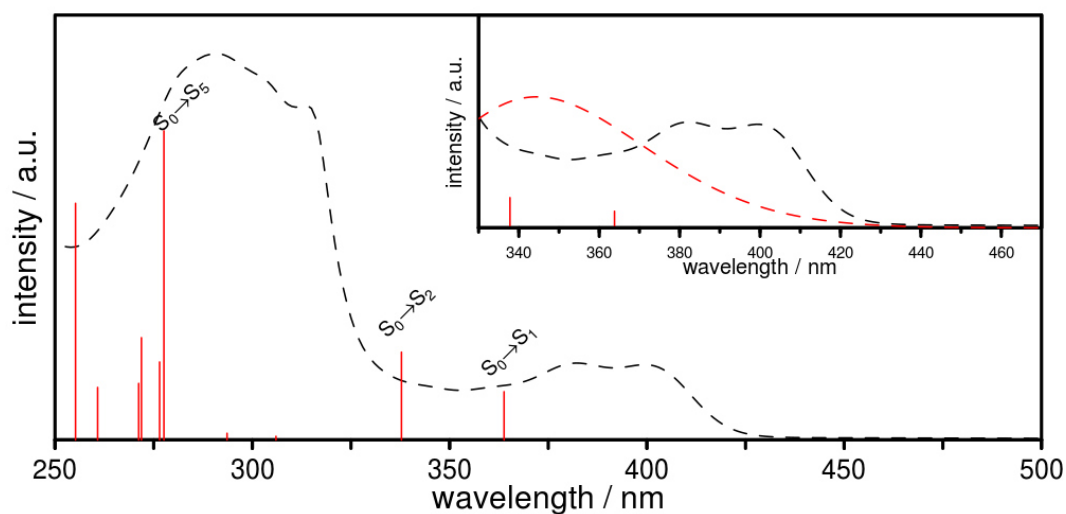
Fig. S22. Normalized UV/vis absorption spectrum of **L2** in acetonitrile (black, dashed) and calculated lowest-lying singlet excitation energies (red vertical lines). The inset represents an enlargement of the region with the lowest lying $\pi \rightarrow \pi^*$ transitions with a simulated spectrum (red, dashed) as summation of gaussians centered at each excitation energy and weighted with their respective oscillator strength. The corresponding calculations for **L1** yield similar results but are omitted because no experimental data for **L1** could have been acquired due to a limited solubility in acetonitrile.
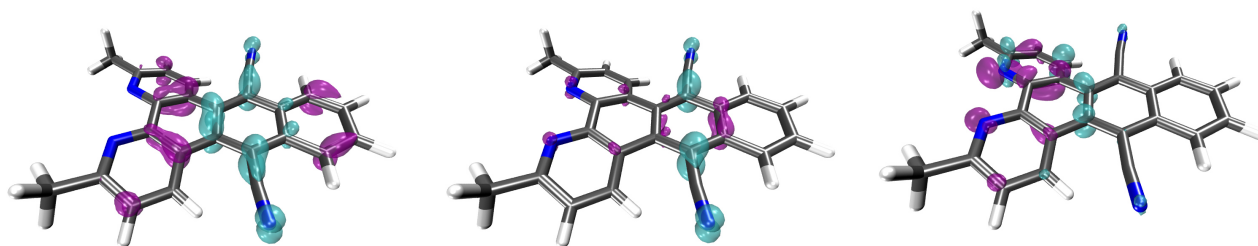
Fig. S23. Differential electron density plots of **L2** between the ground and first excited state (left) and the differential electron density for the $S_0 \rightarrow S_2$ (middle) and $S_0 \rightarrow S_5$ transition (right) in **L2.**

8   Nanosecond Transient Absorption Spectra of 1 and 2
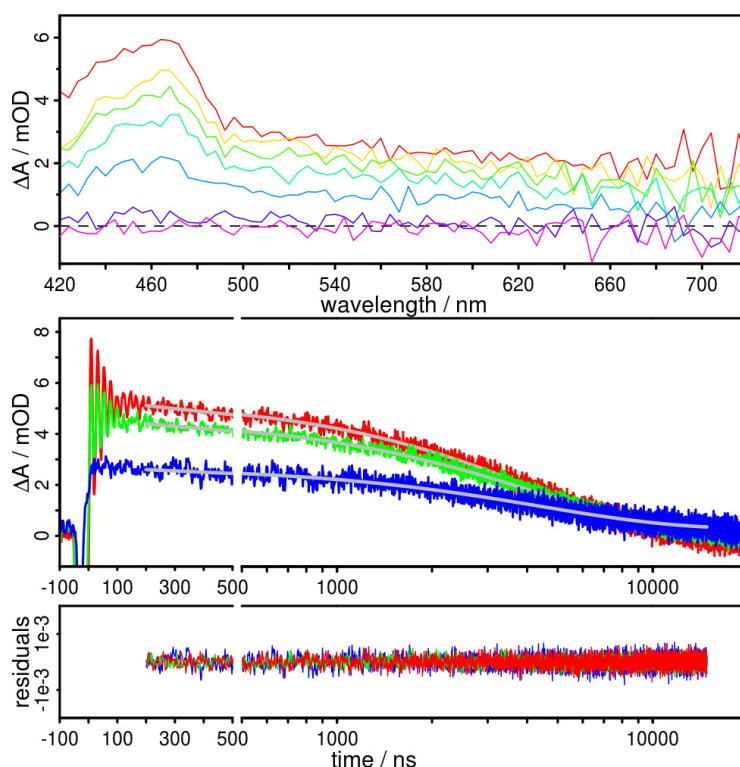
Fig. S24. Transient absorption spectra (top) of **1** in acetonitrile excited at 355 nm after 80 (red), 500 (yellow), 1000 (green), 2000 (cyan), 4000 (blue), 10000 (purple), and 15000 ns (magenta) and kinetics (bottom) with their respective mono-exponential fits at 460 (red), 480 (green) and 600 nm (blue) with τ_1 = **4380 ns.**
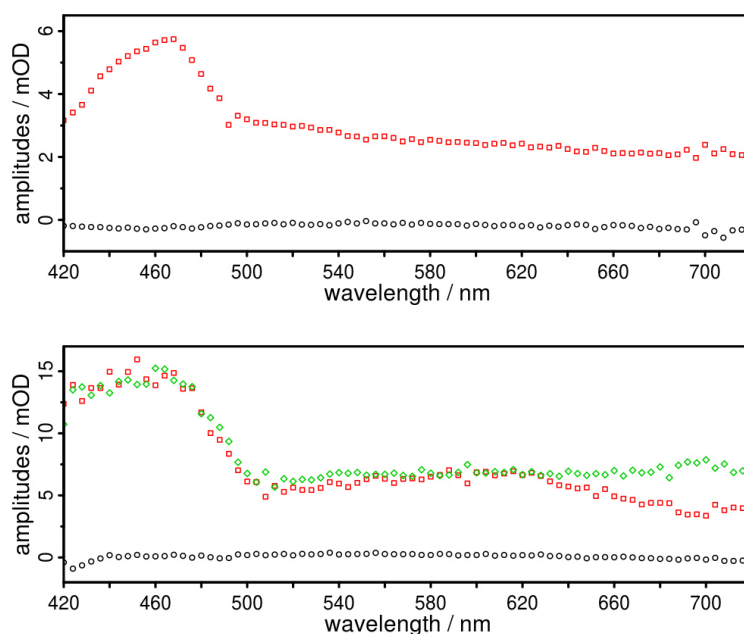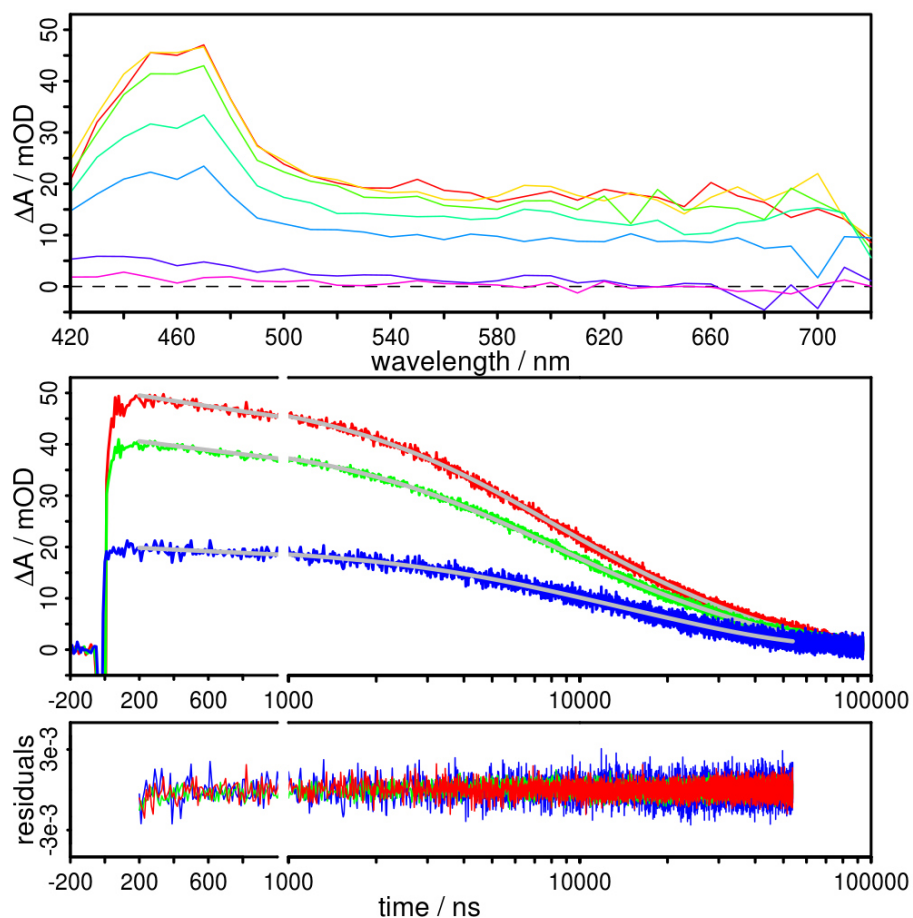

Fig. S25. Decay-associated spectra of the global analysis applied to the transient absorption data ΔOD of **1** (top) and **2** (bottom). The amplitudes of the mono-exponential fit function $F(\lambda, t) = \sum_i^1 c_i(\lambda) \cdot exp(-t/\tau_i) + c_0$ are displayed in red (c_1, first time constant, τ_1 = 4380 ns (**1**) and , τ_1 = 1250 ns (**2**)), green (c_2, second time, τ_2 = 3785 ns (**2**)) and in black (c_0, long-living component).

Fig. S26. Transient absorption spectra (top) of **L2** in acetonitrile excited at 355 nm after 40 (red), 200 (yellow), 1000 (light green), 2000 (dark green), 5000 (cyan), 10000 (blue), 50000 (purple) and 80000 ns (magenta) and kinetics (bottom) with their respective bi-exponential fits at 460 (red), 480 (green) and 600 nm (blue) with τ_1 = 5120 ns and τ_2 = 22180 ns.

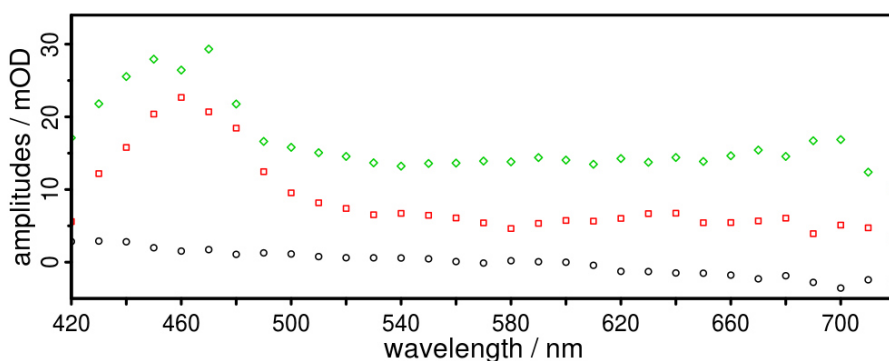**Fig. S27.** Decay-associated spectra of the global analysis applied to the transient absorption data ΔOD of **L2**. The amplitudes of the bi-exponential fit function $F(\lambda, t) = \sum_i^2 c_i(\lambda) \cdot exp(-t/\tau_i) + c_0$ are displayed in red (c_1, first time, τ_1 = 5120 ns), green (c_2, second time, τ_2 = 22180 ns) and in black (c_0, long-living component).
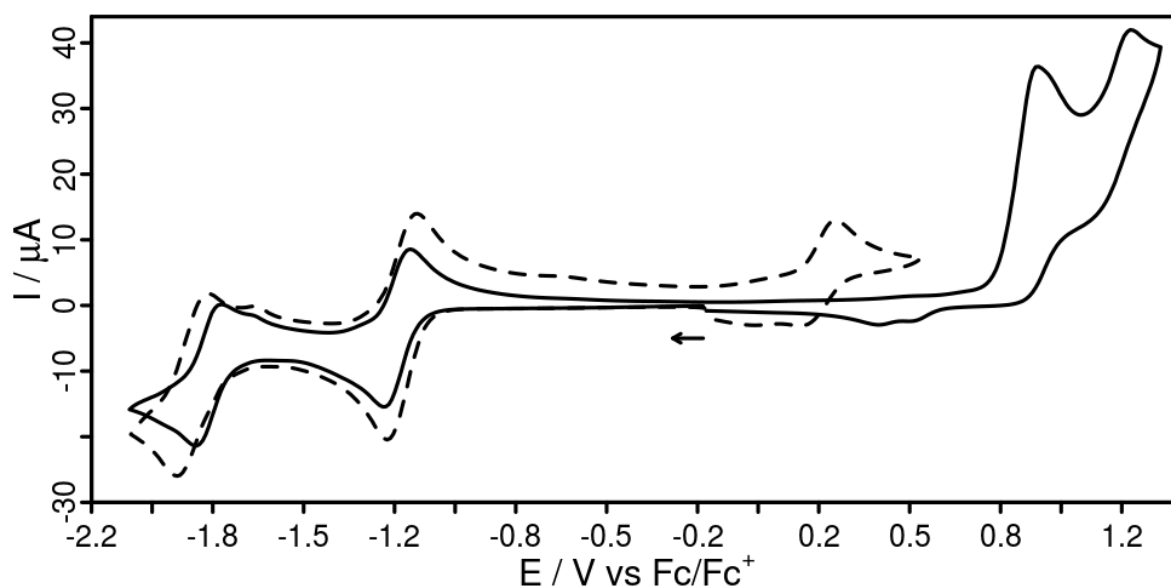
9   Cyclic Voltammograms

Fig. S28. Cyclic voltammogram of **2** (solid) in acetonitrile and **2'** (dashed) in dimethylformamide solution with 0.1 M Bu₄NPF₆ as supporting electrolyte at a scan rate of 100 mV/s and referenced *vs.* the ferrocene/ferrocenium couple. Although complex **2** possesses a P^P ligand (xantphos) instead of a second N^N ligand (**L2**), the ligand-based reduction potentials which are centered on **L2** are almost identical.

Furthermore, there is only a small shift to slightly more cathodic potentials in the case of **2'** compared to **2**. Please note, that the homoleptic Cu(I) complex **2'** was measured in dimethylformamide solution due to its insufficient solubility in acetonitrile. Therefore, this small shift might be only a solvent induced effect.
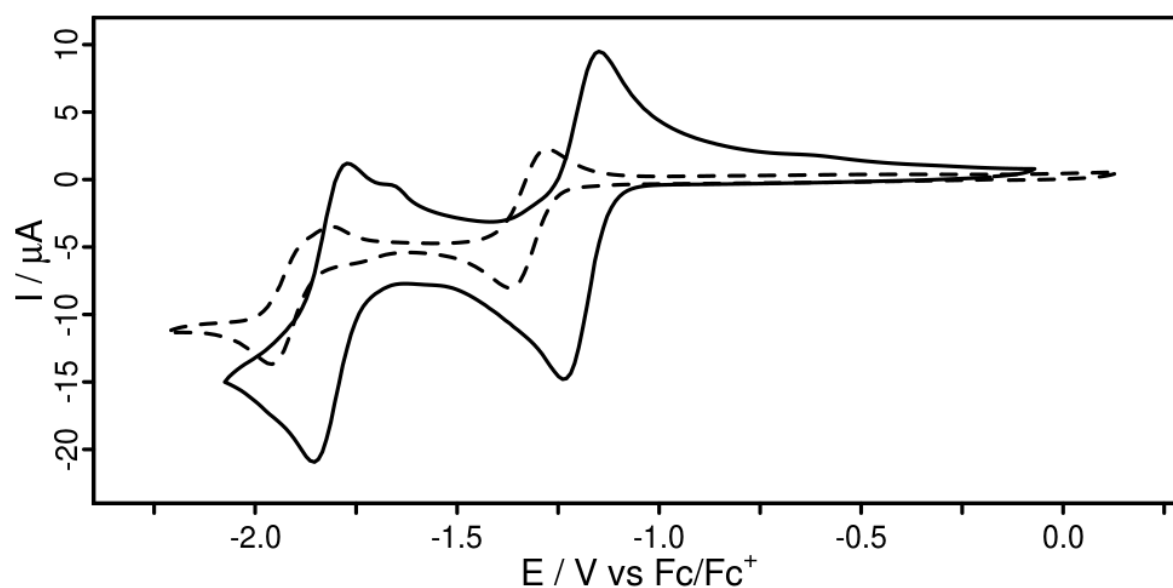

Fig. S29. Cyclic voltammogram of **2** (solid) and **L2** (dashed) in acetonitrile solution with 0.1 M Bu₄NPF₆ as supporting electrolyte at a scan rate of 100 mV/s and referenced *vs.* the ferrocene/ferrocenium couple.
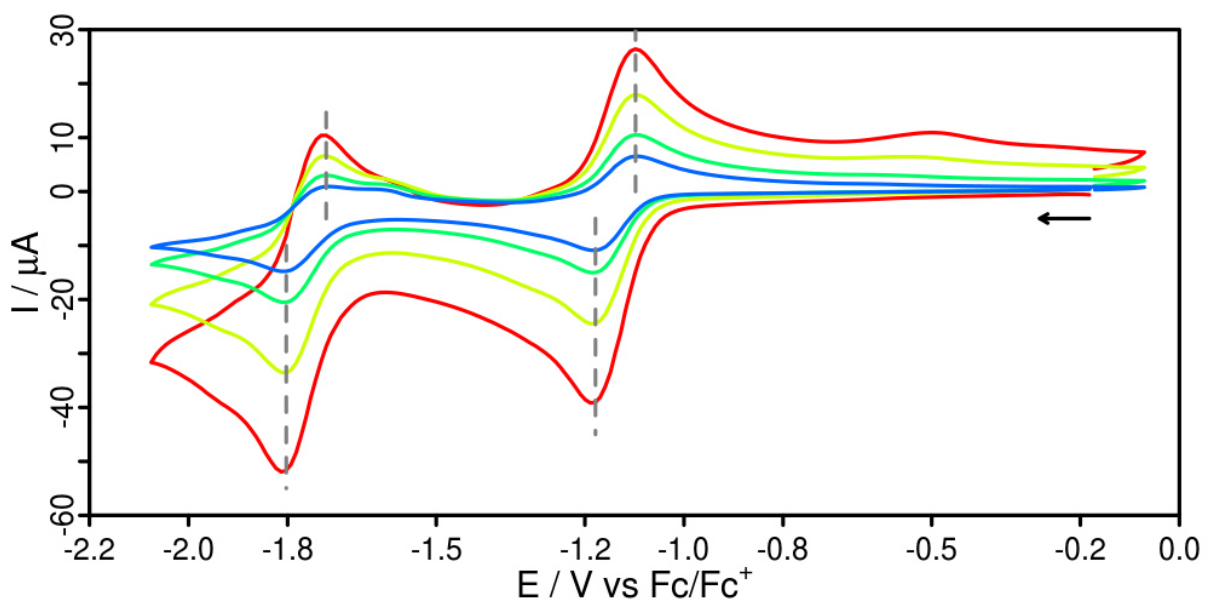
Fig. S30. Cyclic voltammogram of **1** in acetonitrile with 0.1 M Bu₄NPF₆ as supporting electrolyte at different scan rates and referenced *vs.* the ferrocene/ferrocenium couple (blue: 50 mV/s, green: 100 mV/s, yellow: 250 mV/s, red: 500 mV/s). The dashed lines are the peak potentials at a scan speed of 100 mV/s, highlighting the reversibility of the reduction processes.
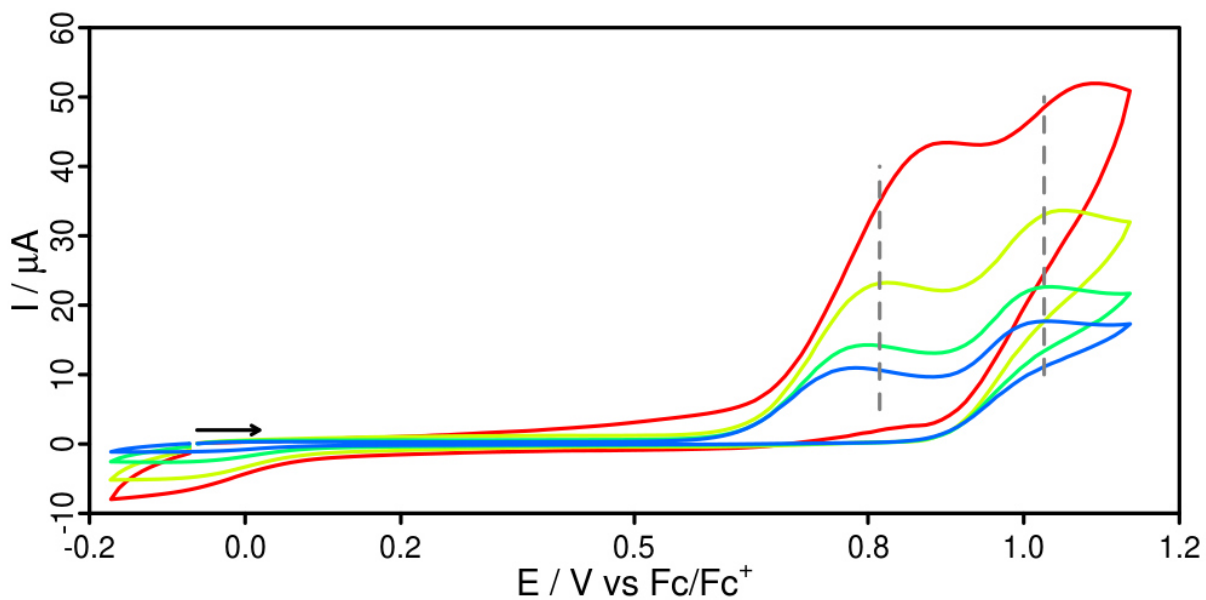

Fig. S31. Cyclic voltammogram of **1** in acetonitrile with 0.1 M Bu₄NPF₆ as supporting electrolyte at different scan rates and referenced *vs.* the ferrocene/ferrocenium couple (blue: 50 mV/s, green: 100 mV/s, yellow: 250 mV/s, red: 500 mV/s). The dashed lines at the peak potentials at a scan speed of 100 mV/s indicate, that the oxidation processes are irreversible.
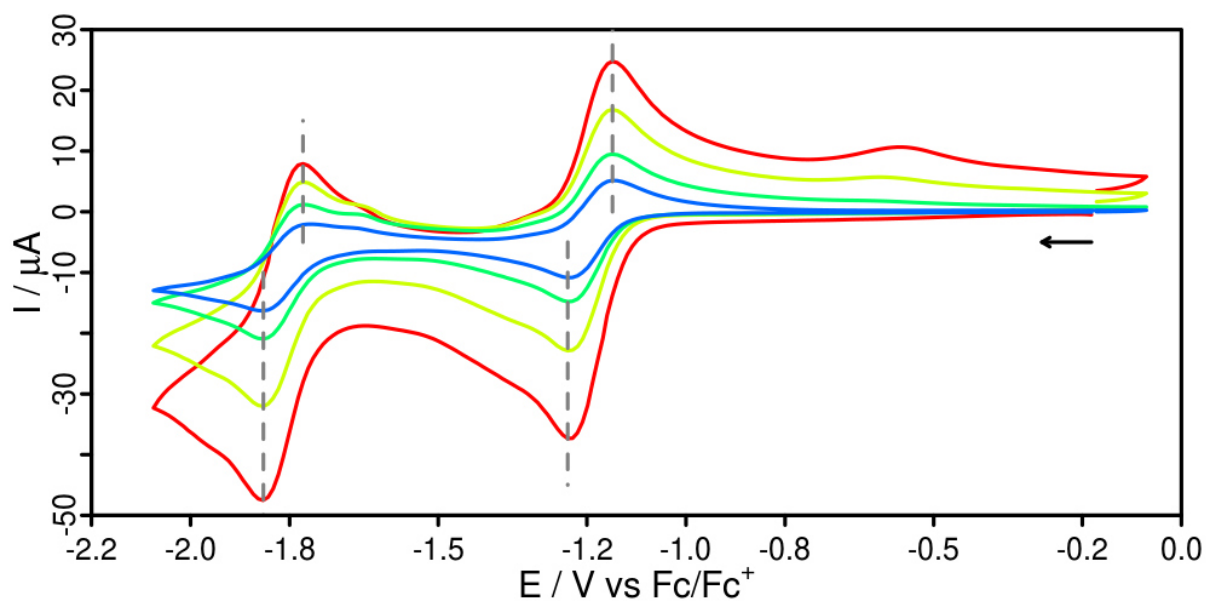
Fig. S32. Cyclic voltammogram of **2** in acetonitrile at different scan speeds (blue: 50 mV/s, green: 100mV/s, yellow: 250mV/s, red: 500mV/s). The dashed lines are the peak potentials at a scan speed of 100mV/s, highlighting the reversibility of the reduction processes.
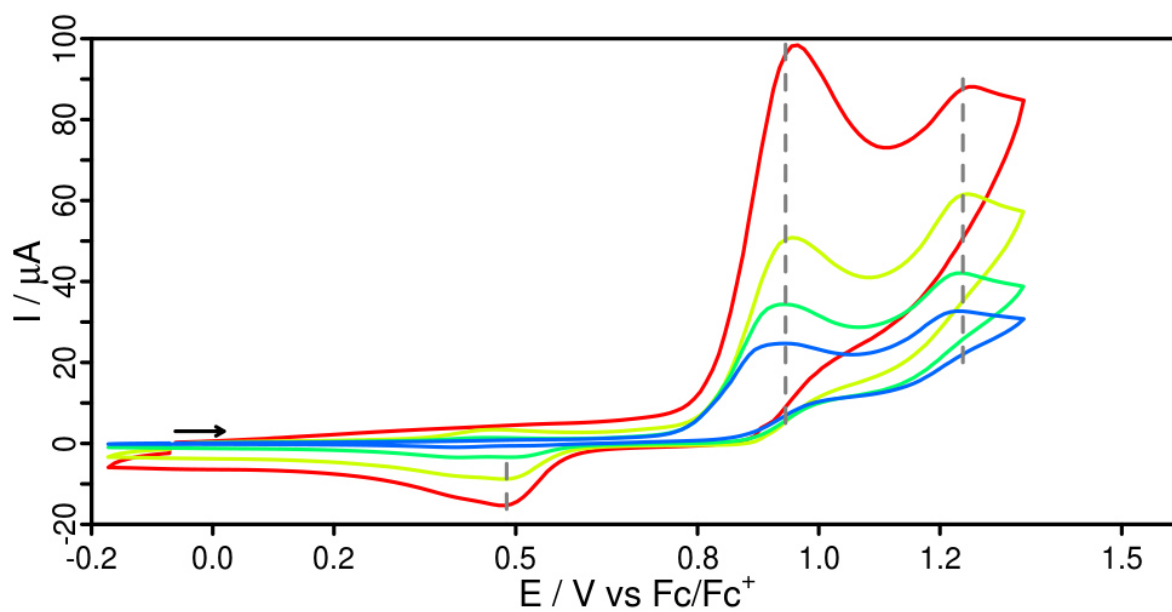

Fig. S33. Cyclic voltammogram of **2** in acetonitrile at different scan speeds (blue: 50 mV/s, green: 100 mV/s, yellow: 250 mV/s, red: 500 mV/s). The dashed lines are the peak potentials at a scan speed of 100 mV/s indicate, that the oxidation processes are irreversible.
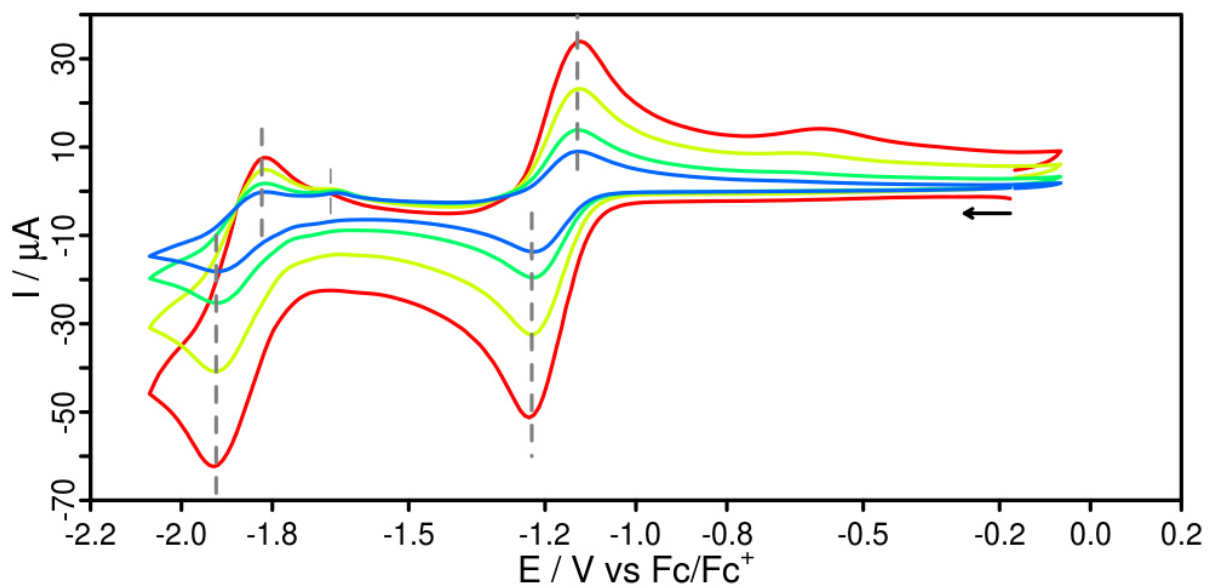
Fig. S34. Cyclic voltammogram of **2'** in acetonitrile at different scan speeds (blue: 50 mV/s, green: 100 mV/s, yellow: 250 mV/s, red: 500 mV/s). The dashed lines are the peak potentials at a scan speed of 100mV/s, highlighting the reversibility of the reduction processes.
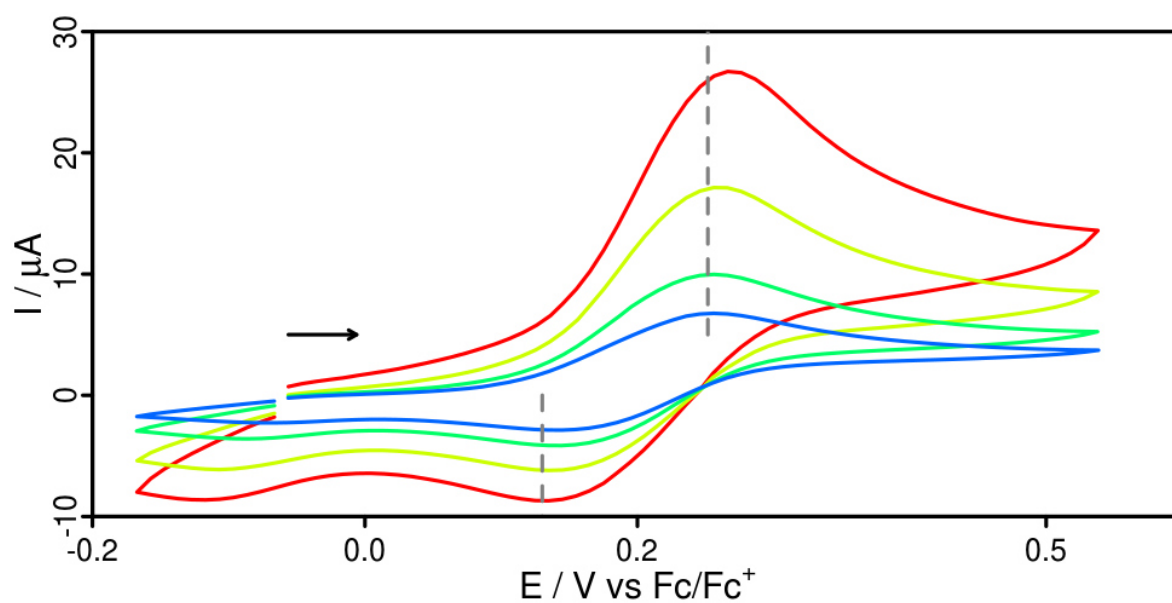

Fig. S35. Cyclic voltammogram of **2'** in acetonitrile at different scan speeds (blue: 50 mV/s, green: 100 mV/s, yellow: 250mV/s, red: 500mV/s). The dashed lines are the peak potentials at a scan speed of 100 mV/s.
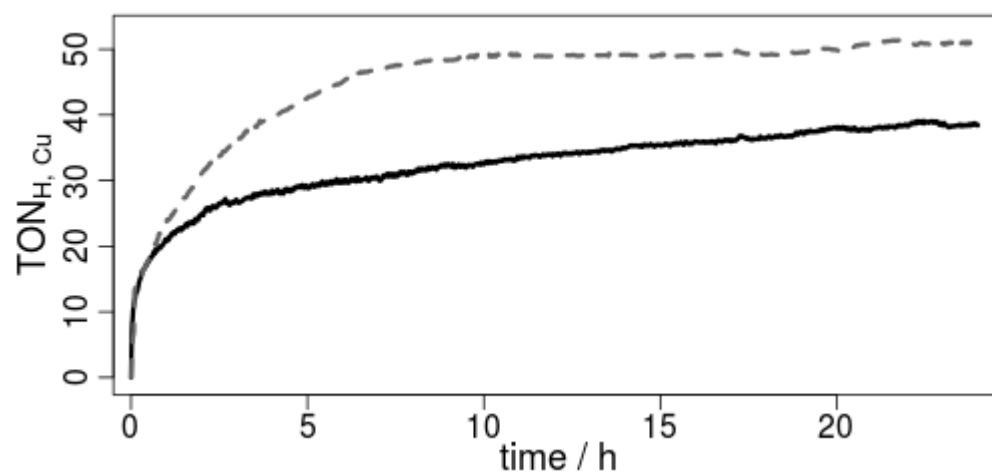
10 Photocatalytic Measurements

Figure SI36. Catalytic activity for light-driven hydrogen production of **1** (black solid) and **2** (dark gray dashed) expressed as turnover number (TON$_{H,Cu}$). Conditions: CuPS (ca. 3.5 μmol), [Fe$_3$(CO)$_{12}$] (ca. 5.0 μmol), in a mixture of THF/TEA/H$_2$O (4:3:1, 10 mL), at 25°C, under Xe light irradiation (output 1.5 W) without light filter, 24 h reaction time. TON$_{H,Cu}$ = n(H) / n(CuPS) with V$_{m,H2,25°C}$ = 24.48 mL/mmol.